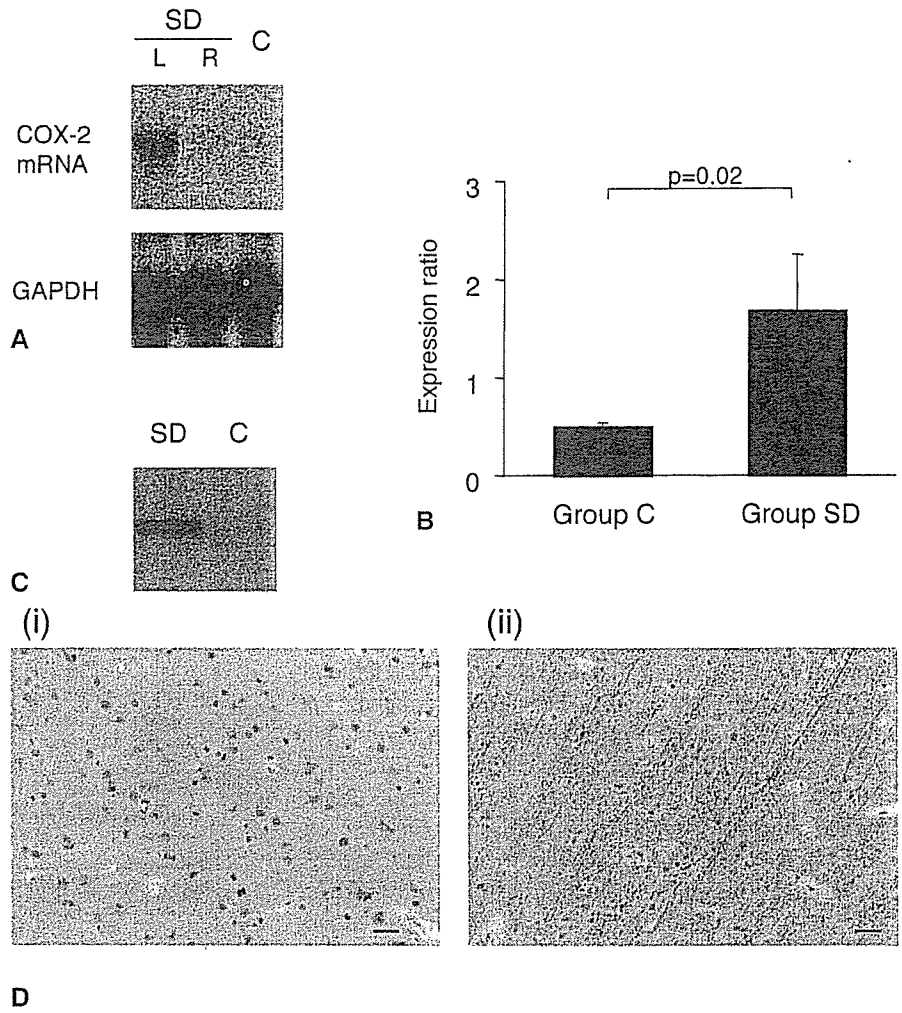

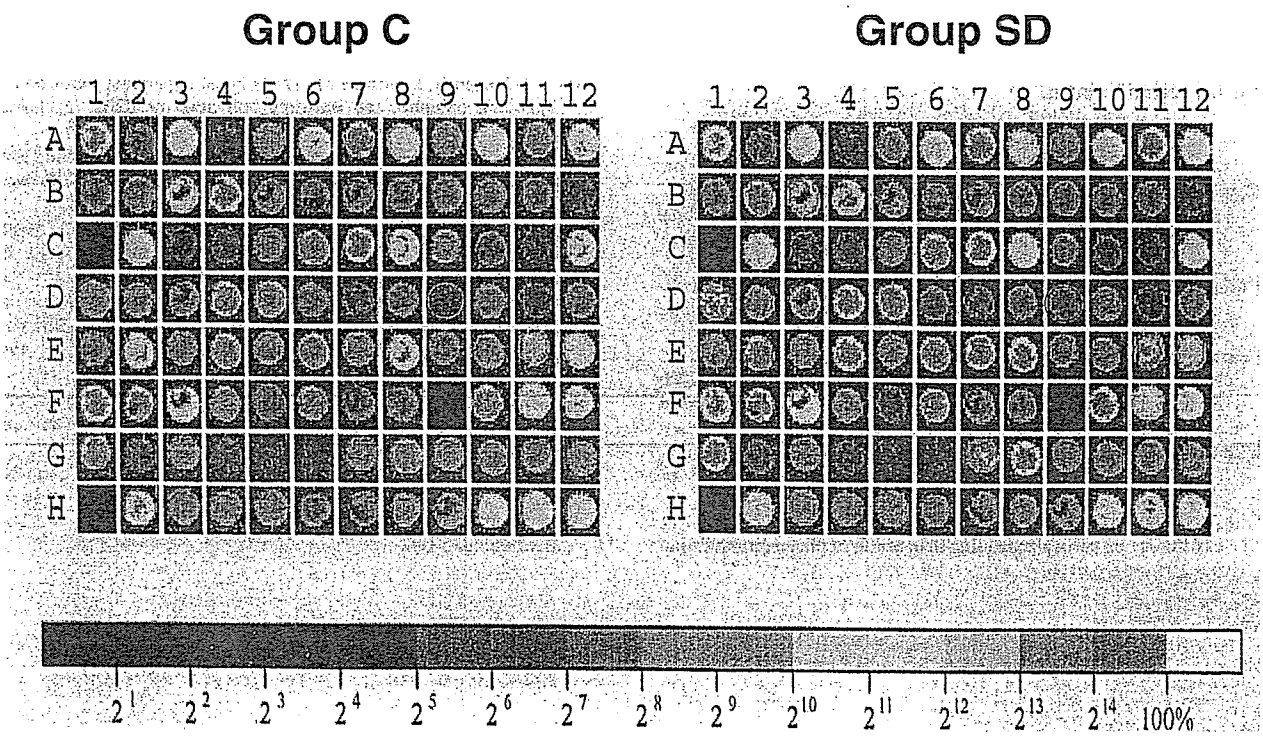

FIG. 1. Cyclooxygenase-2 (COX-2) expression in the primate brain. **(A)** Autoradiograms of COX-2 (top) and glyceraldehyde-3-phosphate dehydrogenase (GAPDH) messenger RNA (bottom) from normal (group C) and spreading depression (SD) animals (group SD). Note that induced COX-2 expression was prominent in the left cortical samples (ipsilateral to the side in which SD was induced). COX-2 expression in the contralateral cortices and in control samples (group C) was faint. **(B)** Expression ratios of COX-2 in each group. The expression ratio of the cortex ipsilateral to the cortex in which SD was induced was significantly higher than that measured in group C ($P = 0.02$). **(C)** Immunoblot analysis revealed a 70- to 72-kd COX-2–immunoreactive band that is clearly seen in the SD group but that is barely detectable in group C. **(D)** Mirror section images immunostained for COX-2 (i) and microtubule-associated protein 2 (MAP-2; ii) are shown. Immunoreactive COX-2 and MAP-2 were localized in the same neurons; cell bodies and apical dendrites showed immunoreactivity. Scale bars: 200 μm.

Nogawa et al., 1997) and that prevention of COX-2 expression might be beneficial in treating human ischemic stroke. Ischemia-related SDs have been regarded as good targets for pharmacologic intervention in stroke because they exacerbate the preexisting energy depletion in the periinfarct zone (Hossmann, 1994; Takano et al., 1996). Cyclooxygenase-2 was induced after SD and as a result of focal brain ischemia in rat models (Koistinaho et al., 1999; Miettinen et al., 1997). Koistinaho and Chan (2000) reported that SD directly induced COX-2 expression in focal brain ischemia by stimulating the NMDA receptor and activating phospholipase A_2. Only a few postmortem studies, however, reported COX-2 expression in human brain ischemia (Iadecola et al., 1999; Sairanen et al., 1998).

In our study, COX-2 was induced in the cortices that experienced SD, supporting previous observations in rodents (Koistinaho et al., 1999; Miettinen et al., 1997). Cyclooxygenase-2 gene expression increased by 1.6-fold in the SD group, as detected using a DNA microarray. The gene transcribing basic transcription element–binding protein 1, a thyroid hormone–regulated gene found in the developing rat brain, was also upregulated (Cayrou et al., 2002); the relation between this protein and SD remains to be clarified. Enard et al. (2002) showed numerous quantitative differences in gene expression between closely related mammalian species. Because they showed that such differences were particularly pronounced in the human brain, primate cDNA arrays analysis will need to be improved before we can fully identify candidate genes that may be involved in SD. In summary, as in rodents, neuronal COX-2 is induced in the primate cortex in response to SD.

Acknowledgments: The authors thank Dr. Toshiho Ohtsuki for his scientific input.

REFERENCES

Cayrou C, Denver RJ, Puymirat J (2002) Suppression of the basic transcription element–binding protein in brain neuronal cultures inhibits thyroid hormone-induced neurite branching. *Endocrinology* 143:2242–2249

Collaco-Moraes Y, Aspey B, Harrison M, Belleroche JD (1996) Cyclooxygenase-2 messenger RNA induction in focal cerebral ischemia. *J Cereb Blood Flow Metab* 16:1366–1372

Enard W, Khaitovich P, Klose J, Zollner S, Heissig F, Giavalisco P, Niselt-Struwe K, Muchmore E, Varki A, Ravid R, Doxiadis GM, Bontrop RE, Paabo S (2002) Intra- and interspecific variation in primate gene expression patterns. *Science* 296:340–343

Gidlund M, Orn A, Pattengale PK, Jansson M, Wigzell H, Nilsson K (1981) Natural killer cells kill tumor cells at a given stage of differentiation. *Nature* 292:848–850

Gill R, Andine P, Hillered L, Persson L, Hagberg H (1992) The effect of MK-801 on cortical spreading depression in the penumbral zone following focal ischemia in the rat. *J Cereb Blood Flow Metab* 12:371–379

Hossmann KA (1994) Viability thresholds and the penumbra of focal ischemia. *Ann Neurol* 36:557–565

Iadecola C, Forster C, Nogawa S, Clark HB, Ross ME (1999) Cyclooxygenase-2 immunoreactivity in the human brain following cerebral ischemia. *Acta Neuropathol* 98:9–14

Iijima T, Mies G, Hossmann KA (1992) Repeated negative DC deflections in rat cortex following middle cerebral artery occlusion are abolished by MK-801: effect on volume of ischemic injury. *J Cereb Blood Flow Metab* 12:727–733

Inoue H, Yokoyama C, Hara S, Tone Y, Tanabe T (1995) Transcriptional regulation of human prostaglandin-endoperoxide synthase-2 gene by lipopolysaccharide and phorbol ester in vascular endothelial cells. *J Biol Chem* 270:24965–24971

Koistinaho J, Chan PH (2000) Spreading depression-induced cyclooxygenae-2 expression in the cortex. *Neurochem Res* 25:645–651

Koistinaho J, Pasonen S, Yrjanheikki J, Chan PH (1999) Spreading depression-induced gene expression is regulated by plasma glucose. *Stroke* 30:114–119

Kuge Y, Hasegawa Y, Yokota C, Minematsu K, Hashimoto N, Miyake Y, Yamaguchi T (2000) Effects of single and repetitive spreading depression on cerebral blood flow and glucose metabolism in cats: a PET study. *J Neurol Sci* 176:114–123

Lauritzen M, Jorgensen MB, Diemer NH, Gjedde A, Hansen AJ (1982) Persistent oligemia of rat cerebral cortex in the wake of spreading depression. *Ann Neurol* 12:469–474

Lauritzen M, Olsen TS, Lassen NA, Paulson OB (1983) Changes in regional cerebral blood flow during the course of classic migraine attacks. *Ann Neurol* 13:633–641

Lyer VR, Eisen MB, Ross DT, Schuler G, Moore T, Lee JCF, Trent JM, Staudt LM, Hudson J, Boguski MS, Lashkari D, Shalon D, Botstein D, Brown PO (1999) The transcriptional program in the response of human fibroblasts to serum. *Science* 283:83–87

Miettinen S, Fusco FR, Yrjanheikki J, Keinanen R, Hirvonen T, Roivainen R, Narhi M, Hokfelt T, Koistinaho J (1997) Spreading depression and focal brain ischemia induce cyclooxygenase-2 in cortical neurons through *N*-methyl-D-aspartic acid-receptors and phospholipase A_2. *Proc Natl Acad Sci U S A* 94:6500–6505

Niwa K, Araki E, Morham SG, Ross ME, Iadecola C (2000) Cyclooxygenase-2 contributes to functional hyperemia in whisker-barrel cortex. *J Neurosci* 20:763–770

Nogawa S, Zhang F, Ross ME, Iadecola C (1997) Cyclo-oxygenase-2 gene expression in neurons contributes to ischemic brain damage. *J Neurosci* 17:2746–2755

Olesen J, Larsen B, Lauritzen M (1981) Focal hyperemia followed by spreading oligemia and impaired activation of rCBF in classic migraine. *Ann Neurol* 9:344–352

Piper RD, Lambert GA, Duckworth JW (1991) Cortical blood flow changes during spreading depression in cats. *Am J Physiol* 261:H96–H102

Sairanen T, Ristimaki A, Karjalainen-Lindsberg M-L, Paetau A, Kaste M, Lindsberg PJ (1998) Cyclooxygenase-2 induced globally in infarcted human brain. *Ann Neurol* 43:738–747

Takano K, Latour LL, Formato JE, Carano RAD, Helmer KG, Hasegawa Y, Sotak CH, Fisher M (1996) The role of spreading depression in focal ischemia evaluated by diffusion mapping. *Ann Neurol* 39:308–318

Woods RP, Iacoboni M, Mazziotta JC (1994) Bilateral spreading cerebral hypoperfusion during spontaneous migraine headache. *New Engl J Med* 331:1689–1692

Yokota C, Kuge Y, Hasegawa Y, Tagaya M, Abumiya T, Ejima N, Tamaki N, Yamaguchi T, Minematsu K (2002) Unique profile of spreading depression in a primate model. *J Cereb Blood Flow Metab* 22:835–842

ELSEVIER

Neuroscience Letters 341 (2003) 37–40

Neuroscience Letters

www.elsevier.com/locate/neulet

Post-ischemic cyclooxygenase-2 expression is regulated by the extent of cerebral blood flow reduction in non-human primates

Chiaki Yokota[a,*], Yuji Kuge[b,c], Hiroyasu Inoue[d], Masafumi Tagaya[e], Go Kito[f], Teruo Susumu[f], Nagara Tamaki[g], Kazuo Minematsu[h]

[a]*Cerebrovascular Laboratory, National Cardiovascular Center Research Institute, 5-7-1 Fujishirodai, Suita, 565-8565, Japan*
[b]*Department of Tracer Kinetics, Graduate School of Medicine, Hokkaido University, Nishi 7, Kita-15, Kita-ku, Sapporo, 060-8638, Japan*
[c]*Institute for Biofunctional Research Co., Inc, 5-7-1 Fujishirodai, Suita, 565-0873, Japan*
[d]*Division of Molecular Pharmacology, Department of Pharmacology, National Cardiovascular Center Research Institute, 5-7-1 Fujishirodai, Suita, 565-8565, Japan*
[e]*Department of Medicine, National Osaka Hospital, 2-1-14, Houenzaka, Chuoku, Osaka, 540-0006, Japan*
[f]*Shin Nippon Biomedical Laboratories, Ltd., 2438, Miyanoura, Yoshidacho, Kagoshima-gun, Kagoshima, 891-1305, Japan*
[g]*Department of Nuclear Medicine, Graduate School of Medicine, Hokkaido University, Nishi 7, Kita-15, Kita-ku, Sapporo, 060-8638, Japan*
[h]*Cerebrovascular Division, Department of Medicine, National Cardiovascular Center, 5-7-1 Fujishirodai, Suita, 565-8565, Japan*

Received 17 December 2002; received in revised form 22 January 2003; accepted 24 January 2003

Abstract

We determined whether up to 24 h of ischemia could induce the expression of cyclooxygenase-2 (COX-2) in the brain of nonhuman primates. Randomized animals were subjected to either a 2 h ischemia (group II; $n = 3$) or a 24 h ischemia (group III; $n = 3$). Three animals in group I served as controls. In group III, regional cerebral blood flow (CBF) and the cerebral glucose metabolic rate (CMRglc) were evaluated using positron emission tomography. Upregulation of COX-2 mRNA expression was observed after 2 h of ischemia, but disappeared by 24 h in the ischemic temporal cortex, in which both CMRglc and CBF were markedly reduced. In the ischemic parietal cortex, where CMRglc was preserved, COX-2 expression persisted even 24 h after ischemia. This study is the first to demonstrate neuronal COX-2 induction within potentially viable hypoperfused brain areas in nonhuman primates.
© 2003 Elsevier Science Ireland Ltd. All rights reserved.

Keywords: Cyclooxygenase-2; Focal brain ischemia; Positron emission tomography; Primate; Cerebral blood flow; Cerebral glucose metabolic rate

Cyclooxygenase-2 (COX-2) is expressed in the brain in discrete neuronal populations in the cortex in response to activation of *N*-methyl-D-aspartate (NMDA) receptors [13]. Several reports, using various rodent models, suggested that COX-2 played role in the development of ischemic injury during focal brain ischemia [1,10]. Supporting these data are the findings in COX-2 deficient mice of a significant reduction in brain injury that was produced by occlusion of the middle cerebral artery, compared to control animals [4]. While these data support the notion that COX-2 inhibition might represent a possible therapeutic target for ischemic stroke, it is still not clear from the few postmortem studies that have been reported [3,11], whether COX-2 is expressed during the acute phase of a stroke. To begin to address this question, we developed a primate model of thromboembolic stroke [7] in which we measured serial changes in cerebral blood flow (CBF) before and after arterial occlusion using positron emission tomography (PET) [8]. The temporal cortex and basal ganglia ipsilateral to the arterial embolization were regarded as the ischemic core, while the ipsilateral parietal cortex was regarded as the peri-infarct area where CBF-cerebral glucose metabolic rate (CMRglc) uncoupling was observed 24 h after embolization. In this paper, we examined the topography and temporal profile of COX-2 expression within 24 h of ischemia in a primate model of thromboembolic stroke using high-resolution PET.

Nine adult male cynomolgus monkeys weighing 3.4–4.3 kg were used in this study. All procedures were approved by our Institutional Animal Care and Use Committee, and were performed in accordance with the standards published by

* Corresponding author. Tel.: +81-6-6833-5012; fax: +81-6-6872-8091.
E-mail address: cyokota@ri.ncvc.go.jp (C. Yokota).

0304-3940/03/$ - see front matter © 2003 Elsevier Science Ireland Ltd. All rights reserved.
doi:10.1016/S0304-3940(03)00152-6

the National Research Council (Guide for the Care and Use of Laboratory Animals). Permanent focal ischemia was produced by carotid arterial embolization as previously described [7]. The monkeys were randomized into three groups of three animals. Animals in group I (normal control) did not undergo arterial embolization. Animals in group II underwent permanent focal ischemia for 2 h, while those in group III underwent permanent focal ischemia for 24 h. COX-2 expression in postmortem brains obtained from each group was investigated by biochemical means. In group III, CBF and the CMRglc were evaluated using high-resolution PET. Each animal was anesthetized by sevoflurane inhalation [0.5–2.0% sevoflurane delivered in a N_2O/O_2 (70%/30%) gas mixture] and was artificially ventilated. Body temperature was monitored and maintained at around 37 °C with the aid of heating pads.

The PET studies were performed with a multi-slice PET scanner (ECAT EXACT HR/47, Siemens/CTI, Knoxville, TN) [12], which provided 47 tomographic images at 3.1 mm intervals per frame. The spatial resolution at the center of the field of view was 3.7 mm in-plane at full width at half maximum and 4.1 mm axially. CBF and CMRglc were determined using ^{15}O-labeled water (^{15}O-H_2O) and 2-[^{18}F]fluoro-2-deoxy-D-glucose, respectively, and data analysis was performed according to the methods described previously [8]. To control for potential problems that arise as a result of the repeated withdrawal of blood during prolonged periods of experimentation, as a result of the effects associated with variations in levels of anesthesia, and as a result of partial volume effects [2], we expressed our results in terms of asymmetry index (AI), which was defined as the ratio of the value of regional CBF in the ROIs in the ischemic hemisphere to that in the contralateral homologous ROIs.

All animals were sacrificed by exsanguination following perfusion with ice-cold saline under pentobarbital anesthesia. Each brain was quickly removed and stereotaxically divided on ice into three slices corresponding to the coronal PET images as the same manner as the previous study [8]. Samples were extracted from the temporal cortices, parietal cortices, and basal ganglia, the size of which were 1 × 1 cm (width × height; Fig. 1A). Each sample was subdivided into two 4 mm (depth) pieces, which were dissected out from each slice from both ischemic and non-ischemic temporal lobe sections – one piece (>60 mg) was used for biochemical examination while the other was used for histopathological analysis.

RNA blot analysis was performed as previously described [6]. Total RNAs were prepared from samples derived from the second slice from both sides of animals in each group. In one animal in group II, total RNAs were also prepared from samples in each of the three slices from the ischemic side. The amount of COX-2 mRNA in each region was expressed as the ratio of the COX-2 mRNA signal to the glyceraldehyde-3-phosphate dehydrogenase (GAPDH) mRNA signal in that region (expression ratio).

Paraffin-embedded brain sections (3 μm thick), which

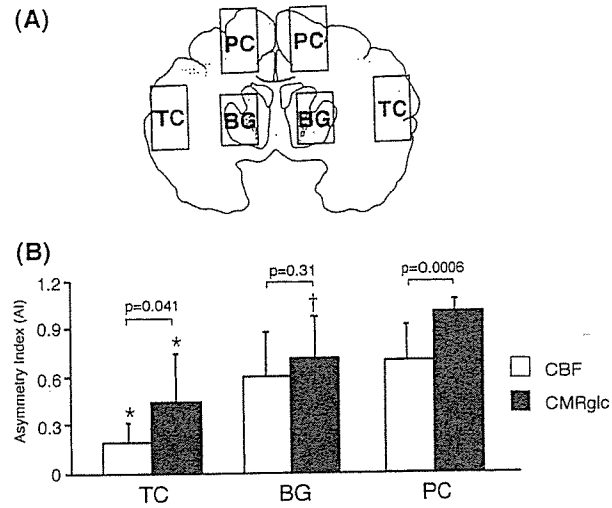

Fig. 1. (A) Manner of sample preparation. The brain was stereotaxically divided on ice into three slices corresponding to coronal PET images: the first rostral slice was a coronal cut at 23 mm from the frontal pole and another two slices were cut at 9 mm intervals parallel to the first slice. From each slice, both the ischemic and the non-ischemic temporal cortices (TC), parietal cortices (PC), and the basal ganglia (BG) were dissected out. (B)AIs for CBF and CMRglc following 24 h of focal ischemia. AIs for both CBF and CMRglc in the TC were reduced significantly (*) compared to those in the BG and PC. In the basal ganglia, AIs for CMRglc were also reduced significantly (†) compared to those in the parietal cortex. Results from a two-way analysis of variance that was used to assess the significance of differences in the AIs between CBF and CMRglc were: $P = 0.041$, $P = 0.31$, and $P = 0.0006$ for the temporal cortex, the basal ganglia, and the parietal cortex, respectively.

were taken from the second slice from the ischemic hemispheres in groups II and III, and second slice from the left hemispheres in group I, were deparaffinized and incubated with a polyclonal COX-2 antibody (Cayman Chemical, Ann Arbor, MI; dilution 1:100) for 2 h at room temperature. After sections were washed with phosphate-buffered saline, biotinylated goat serum against rabbit IgG (Vector Laboratories, Burlingame, CA) was applied and the sections were incubated for at least 30 min at 25 °C. Immunoreactive signals were visualized using diaminobenzidine as the chromogen in a peroxidase reaction (Vectastain Elite Kit, Vector Laboratories).

During the PET studies, physiological parameters including mean blood pressure, blood gases, and body temperature were maintained within the normal range. There were no significant differences in AIs for both CBF and CMRglc among the three slices from each site i.e. temporal cortex, parietal cortex, and basal ganglia. Significant reductions in AIs for CBF as well as CMRglc were demonstrated in the temporal cortex compared to those in the basal ganglia and parietal cortex (Fig. 1B). In the basal ganglia, AIs for CMRglc were also significantly reduced compared to those in the parietal cortex. On the other hand, the mean AI for CMRglc was preserved in the parietal cortex, whereas the mean AI for CBF was found to be reduced.

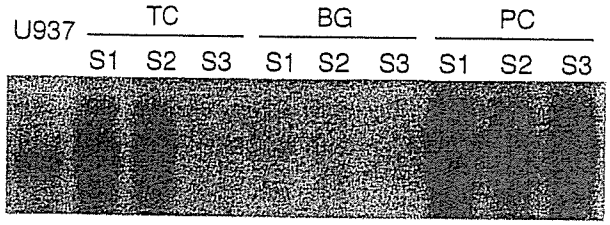

TC: temporal crtex, BG: basal ganglia, PC: parietal cortex
S1: slice 1, S2: slice 2, S3: slice 3

Fig. 2. RNA blot analysis of COX-2 expression following 2 h of ischemia in group II. COX-2 mRNA expression was detected in each region from the ischemic side. COX-2 mRNA expression in the ischemic parietal cortex was prominent, while expression in the ischemic basal ganglia was faint.

COX-2 mRNA expression following 2 h of ischemia (group II) was detected in each region from the ipsilateral hemisphere (Fig. 2). Expression of COX-2 mRNA in the first (slice1) and second (slice2) slices from the ischemic temporal cortex and in all slices (slice1, slice2, slice3) from the ischemic parietal cortex, was detected specifically as a single band (4.5 kb), the size of which was similar to that of human COX-2 mRNA extracted from lipopolysaccharide-treated U937 cells [5]; expression in the ischemic basal ganglia was faint. Expression of COX-2 mRNA in normal controls (group I) was as low as that on the side contralateral to the arterial embolization (Table 1). Expression ratios of COX-2 mRNA in group II were high in the ipsilateral cortices compared to those in group I. In group III, COX-2 mRNAs were undetectable in the ischemic temporal cortices and there were marked reductions in GAPDH mRNA expression, while expression ratios of COX-2 mRNA in the parietal cortex ipsilateral to the arterial embolization were prominently upregulated to the same levels as those seen in group II. Localized COX-2 immunoreactive neurons were detected predominantly in the ischemic parietal cortex in group III, while a few immunoreactive neurons were also observed in the ischemic temporal cortex and basal ganglia in group II. These immunoreactive neurons showed intense immunoreactivity in their cell bodies and apical dendrites (Fig. 3).

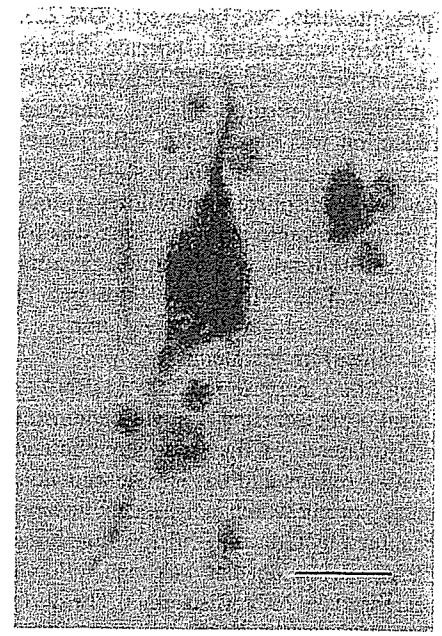

Fig. 3. Induction of COX-2 immunoreactive neurons in the parietal cortex in primate focal ischemia. Scale bar: 100 μm. Neuronal cell bodies and (apical) dendrites showed COX-2 immunoreactivity.

Table 1
Comparison of expression ratios of COX-2 mRNA between the three groups[a]

	Group I	Group II		Group III	
		ipsi	contra	ipsi	contra
Temporal cortex	0.83	11.83	0.69	–	0.60
	0.69	3.41	1.38	–	0.93
	0.45	6.97	1.57	–	0.38
Mean ± SD	0.66 ± 0.19	7.40* ± 4.23	1.21 ± 0.46	–	0.64 ± 0.28
Basal ganglia	0.33	1.03	0.66	–	0.55
	0.84	0.67	0.69	3.88	0.33
	0.13	3.91	0.93	2.07	0.28
Mean ± SD	0.43 ± 0.37	1.87 ± 1.78	0.76 ± 0.15	2.98 ± 1.28	0.39 ± 0.14
Parietal cortex	0.62	5.77	1.02	5.87	1.01
	0.65	4.44	1.49	2.62	0.87
	0.39	4.00	1.11	4.85	0.86
Mean ± SD	0.55 ± 0.14	4.74** ± 0.92	1.21 ± 0.25	4.45** ± 1.67	0.91 ± 0.08

[a] Group I indicates normal control. Animals in group II underwent permanent focal ischemia for 2 h, and those in group III underwent permanent focal ischemia for 24 h. Samples from three animals were used except in group III – ipsilateral (ipsi), basal ganglia – which were derived from only two animals because of a marked reduction in expression of both COX-2 and GAPDH mRNA. COX-2 transcripts were undetectable in all three samples from ipsilateral, temporal cortices in group III (–). A one-way analysis of variance was used to assess the significance of differences in the expression ratios between the three groups. *significantly higher than the temporal cortex in group I and temporal cortices contralateral (contra) to the arterial embolization in groups II and III ($P < 0.05$). **significantly higher than the parietal cortex in group I and parietal cortices contralateral (contra) to the arterial embolization in groups II and III ($P < 0.05$).

In the present study, we observed COX-2 expression during focal brain ischemia in a primate thromboembolic stroke model in which regional CBF and CMRglc were evaluated using high-resolution PET scanning. In this model, a reduction was observed in CBF in the ischemic temporal cortex and basal ganglia to $<40\%$ of the CBF in the contralateral hemisphere 1 h following embolization, while CBF in the ischemic parietal cortex was found to be $>40\%$ of contralateral values; these results support previous findings [7,8]. The flow threshold for infarct development was 12–15 ml $100g^{-1}$ min^{-1} (40% of contralateral values) in this model [8].

Our finding of an increase in COX-2 mRNA expression following focal brain ischemia that was demonstrable in the hemisphere ipsilateral to the arterial embolization, was consistent with previous findings in rodent models [1,9,10]. In the ischemic core in which a significant decrease in CBF were accompanied by reduced CMRglc, the upregulation in COX-2 mRNA expression that was seen following 2 h of ischemia decreased by 24 h of ischemia. The disappearance of COX-2 following 24 h of ischemia paralleled the reduction in expression of mRNA for the house-keeping gene, GAPDH, which indicated that ischemic injury was already apparent at this time in the basal ganglia as well as in the temporal cortex, a finding that is consistent with our previous report [8]. On the other hand, in the peri-infarct area, induced expression of COX-2 mRNA was still present following 24 h of ischemia in the parietal cortex, as was a mild CBF reduction, though CMRglc was maintained. Delayed induction of COX-2 in the infarcted human brain was suggested to promote reconstitutive processes in the form of tissue scarring and remodeling of the surviving neural networks [11]. Although interpretation of the results in this study should be careful because of the limited number of primates, we propose that the regulation of COX-2 expression is different in the ischemic core than in the peri-infarct area, and that therefore the role of COX-2 in focal ischemic tissues is determined by the depth and duration of CBF reduction.

Acknowledgements

We are grateful to Dr Takeo Abumiya for his suggestions concerning the preparation of this manuscript, and thank Mr. Norimasa Ejima and Miss Yumi Miyamoto for their technical assistance. This work was supported in part by Special Coordination Funds for Promoting Science and Technology (Strategic Promotion System for Brain Science) from the Ministry of Education, Culture, Sports, Science and Technology of Japan, by a Grant-in-Aid for Scientific Research from the Japan Society for the Promotion of Science, by a Grant from Japan Heart Foundation Research, by a Grant from the Takeda Medical Research Foundation in Japan, and by Research Grants for Cardiovascular Diseases (11C-3, 12A-2) from the Ministry of Health, Labor and Welfare of Japan.

References

[1] Y. Collaco-Moraes, B. Aspey, M. Harrison, J.D. Belleroche, Cyclo-oxygenase-2 messenger RNA induction in focal cerebral ischemia, J. Cereb. Blood Flow Metab. 16 (1996) 1366–1372.
[2] W.-D. Heiss, R. Graf, K. Wienhard, L.R. Saito, T. Fujita, G. Rosner, R. Wagner, Dynamic penumbra demonstrated by sequential multitracer PET after middle cerebral artery occlusion in cats, J. Cereb. Blood Flow Metab. 14 (1994) 892–902.
[3] C. Iadecola, C. Forster, S. Nogawa, H.B. Clark, M.E. Ross, Cyclooxygenase-2 immunoreactivity in the human brain following cerebral ischemia, Acta. Neuropathol. 98 (1999) 9–14.
[4] C. Iadecola, K. Niwa, S. Nogawa, X. Zhao, M. Nagayama, E. Araki, S. Morham, M.E. Ross, Reduced susceptibility to ischemic brain injury and *N*-methyl-D-aspartate-mediated neurotoxicity in cyclooxygenase-2-deficient mice, Proc. Natl. Acad. Sci. USA 98 (2001) 1294–1299.
[5] H. Inoue, T. Tanabe, K. Umesono, Feedback control of cyclooxygenase-2 expression through PPARgammma, J. Biol. Chem. 275 (2000) 28028–28032.
[6] H. Inoue, C. Yokoyama, S. Hara, Y. Tone, T. Tanabe, Transcriptional regulation of human prostaglandin-endoperoxide synthase-2 gene by lipopolysaccharide and phorbol ester in vascular endothelial cells, J. Biol. Chem. 270 (1995) 24965–24971.
[7] G. Kito, A. Nishimura, T. Susumu, R. Nagata, Y. Kuge, C. Yokota, K. Minematstu, Experimental thromboembolic stroke in cynomolgus monkey, J. Neurosci. Methods 105 (2001) 45–53.
[8] Y. Kuge, C. Yokota, M. Tagaya, Y. Hasegawa, A. Nishimura, G. Kito, N. Tamaki, N. Hashimoto, T. Yamaguchi, K. Minematsu, Serial changes in cerebral blood flow and flow-metabolism uncoupling in primates with acute thromboembolic stroke, J. Cereb. Blood Flow Metab. 21 (2001) 202–210.
[9] S. Miettinen, F.R. Fusco, J. Yrjanheikki, R. Keinanen, T. Hirvonen, R. Roivainen, M. Narhi, T. Hokfelt, J. Koistinaho, Spreading depression and focal brain ischemia induce cyclooxygenase-2 in cortical neurons through *N*-methyl-D-aspartic acid-receptors and phospholipase A2, Proc. Natl. Acad. Sci. USA 94 (1997) 6500–6505.
[10] S. Nogawa, F. Zhang, M.E. Ross, C. Iadecola, Cyclo-oxygenase-2 gene expression in neurons contributes to ischemic brain damage, J. Neurosci. 17 (1997) 2746–2755.
[11] T. Sairanen, A. Ristimaki, M.-L. Karjalainen-Lindsberg, A. Paetau, M. Kaste, P.J. Lindsberg, Cyclooxygenase-2 induced globally in infarcted human brain, Ann. Neurol. 43 (1998) 738–747.
[12] K. Wienhard, M. Dahlbom, L. Eriksson, C. Michel, T. Bruckbauer, U. Pietrzyk, W.D. Heiss, The ECAT EXACT HR: performance of a new high resolution positron scanner, J. Comput. Assist. Tomogr. 18 (1994) 110–118.
[13] K. Yamagata, K.I. Andreasson, W.E. Kaufmann, C.A. Barnes, P.F. Worley, Expression of a mitogen-inducible cyclooxygenase in brain neurons: regulation by synaptic activity and glucocorticoids, Neuron 11 (1993) 371–386.

Article

Activity of Rho-family GTPases during cell division as visualized with FRET-based probes

Hisayoshi Yoshizaki,[1,2] Yusuke Ohba,[1,2] Kazuo Kurokawa,[1] Reina E. Itoh,[1] Takeshi Nakamura,[1] Naoki Mochizuki,[3] Kazuo Nagashima,[2,4] and Michiyuki Matsuda[1]

[1]Department of Tumor Virology, Research Institute for Microbial Diseases, Osaka University, Osaka 565-0871, Japan
[2]Core Research for Evolutional Science and Technology, Japan Science and Technology Cooperation, Fukuoka 816-8580, Japan
[3]Department of Structural Analysis, National Cardiovascular Center Research Institute, Osaka 565-8565, Japan
[4]Laboratory of Molecular and Cellular Pathology, Hokkaido University School of Medicine, Sapporo 060-8638, Japan

Rho-family GTPases regulate many cellular functions. To visualize the activity of Rho-family GTPases in living cells, we developed fluorescence resonance energy transfer (FRET)–based probes for Rac1 and Cdc42 previously (Itoh, R.E., K. Kurokawa, Y. Ohba, H. Yoshizaki, N. Mochizuki, and M. Matsuda. 2002. *Mol. Cell. Biol.* 22:6582–6591). Here, we added two types of probes for RhoA. One is to monitor the activity balance between guanine nucleotide exchange factors and GTPase-activating proteins, and another is to monitor the level of GTP-RhoA. Using these FRET probes, we imaged the activities of Rho-family GTPases during the cell division of HeLa cells. The activities of RhoA, Rac1, and Cdc42 were high at the plasma membrane in interphase, and decreased rapidly on entry into M phase. From after anaphase, the RhoA activity increased at the plasma membrane including cleavage furrow. Rac1 activity was suppressed at the spindle midzone and increased at the plasma membrane of polar sides after telophase. Cdc42 activity was suppressed at the plasma membrane and was high at the intracellular membrane compartments during cytokinesis. In conclusion, we could use the FRET-based probes to visualize the complex spatio-temporal regulation of Rho-family GTPases during cell division.

Introduction

Rho-family GTPases, including Rho (A, B, and C isoforms), Rac (1, 2, and 3 isoforms), and Cdc42, regulate a number of cell functions, including gene expression, cell adhesion, and cell division (Narumiya, 1996; Bishop and Hall, 2000). Earlier analyses using *Xenopus* and sand dollar eggs have shown that Rho and Cdc42 play a particularly essential role in cytokinesis (Kishi et al., 1993; Mabuchi et al., 1993; Drechsel et al., 1997). The importance of Rho in cytokinesis has further been supported by the observations that Rho and its effectors (ROCK and citron) accumulate at the cleavage furrow (Takaishi et al., 1995; Madaule et al., 1998; Kosako et al., 1999), and that cytokinesis is perturbed by the expression of dominant-negative forms of citron and ROCK (Madaule et al., 1998) or by an inhibitor to ROCK (Kosako et al., 2000). It has also been proposed that Rac and Cdc42 are involved in the cytokinesis of mammalian cells, based on the appearance of multinucleated cells among cells expressing constitutively active Rac1 or Cdc42 (Dutartre et al., 1996; Muris et al., 2002).

Rho-family GTPases are regulated by three classes of protein: guanine nucleotide exchange factors (GEFs),* GTPase-activating proteins (GAPs), and guanine nucleotide dissociation inhibitors (GDIs) (Takai et al., 2001). GEF promotes exchange of GDP bound to Rho-family GTPases with GTP, and this exchange causes the Rho-family GTPases to bind to their effector proteins. The GTP-bound active Rho-family GTPases return to the GDP-bound inactive form by GTP hydrolysis, which is strongly promoted by GAP. GDI extracts GDP-bound Rho-family GTPases from membrane compartments and holds them in the cytoplasm (Olofsson, 1999). As expected from the aforementioned role of Rho-family GTPases in cytokinesis, there has been a plethora of reports on the critical

The online version of this article includes supplemental material.

Address correspondence to M. Matsuda, Dept. of Tumor Virology, Institute for Microbial Diseases, Osaka University, Yamadaoka, Suita-shi, Osaka 565-0871, Japan. Tel.: 81-6-6879-8316. Fax: 81-6-6879-8314. E-mail: matsudam@biken.osaka-u.ac.jp

Key words: fluorescent probes; cytokinesis; rho GTP-binding proteins; rac GTP-binding proteins; Cdc42 GTP-binding protein

*Abbreviations used in this paper: FRET, fluorescence resonance energy transfer; GAP, GTPase-activating protein; GDI, guanine nucleotide dissociation inhibitor; GEF, guanine nucleotide exchange factor; RBD, RhoA-binding domain; TPEM, two-photon excitation fluorescence microscopy.

© The Rockefeller University Press, 0021-9525/2003/07/223/10 $8.00
The Journal of Cell Biology, Volume 162, Number 2, July 21, 2003 223–232
http://www.jcb.org/cgi/doi/10.1083/jcb.200212049

Supplemental Material can be found at:
http://www.jcb.org/cgi/content/full/jcb.200212049/DC1

The Journal of Cell Biology

Downloaded from www.jcb.org on July 13, 2006

The Journal of Cell Biology

roles of these regulators in cytokinesis (Prokopenko et al., 2000).

Despite the accumulated knowledge on the involvement of Rho-family GTPases in many intracellular signaling events, their spatio-temporal regulation has not been assessed until recently, mostly due to the difficulty in monitoring their activities. To overcome this difficulty, in vivo probes have been developed based on the principle of fluorescence resonance energy transfer (FRET; Kraynov et al., 2000; Mochizuki et al., 2001; Itoh et al., 2002). FRET is a nonradiative transfer of energy between two fluophores that are placed in close vicinity and in a proper relative angular orientation (Zhang et al., 2002). Variants of GFP have provided genetically encoded fluophores that serve as donor and/or acceptor in FRET (Heim and Tsien, 1996; Mitra et al., 1996; Mizuno et al., 2001). Using these GFP variants and FRET technology, we previously developed genetically encoded probes, called Raichu, for the monitoring of activities of low mol wt GTPases in living cells (Mochizuki et al., 2001; Itoh et al., 2002). Here, we introduce two new Raichu probes, Raichu-RhoA and Raichu-RBD, for the monitoring of RhoA activity. Then, we use these new FRET-based probes to demonstrate that Rho-family GTPases are regulated in a manner dependent on space and time during cell division.

Results

Development of Raichu-RhoA

As a follow-up to our previous probes for Ras-superfamily GTPases, here we developed the probes for RhoA, which generally consisted of truncated RhoA (aa 1–189), the RhoA-binding domain (RBD) of effectors, and a pair of GFP mutants, YFP and CFP (Fig. 1 A). In these probes, the intramolecular binding of GTP-RhoA to the effector protein was expected to bring CFP in closer proximity to YFP, resulting in an increase in FRET from CFP to YFP. We chose mDia, Rhotekin, Rhophilin, and PKN for the RhoA effector proteins, and tested probes with either of the configurations YFP–RhoA–effector–CFP or YFP–effector–RhoA–CFP. The Rac1/Cdc42-binding domain of PAK was used as a negative control. As a typical example, the emission profile of Raichu–RhoA–1237X, which will be described later in detail, is shown in Fig. 1 B. Because FRET was most clearly observed as an increase in an emission peak of YFP at 527 nm and a decrease in an emission peak of CFP at 475 nm, the emission ratio of YFP/CFP is used to demonstrate the FRET efficiency hereafter.

To search for the RhoA effector most suitable for the probe, we prepared a pair of probes carrying either the wild-type or Q63L GTPase-deficient mutant of RhoA for each RhoA effector. Wild-type probes with the effector domain of mDia, Rhotekin, and Rhophilin were found to contain extremely high levels of GTP. Consequently, the FRET efficiency was not markedly different between the wild-type and Q63L mutants of these probes (Table I). We speculate that the RBDs of these proteins inhibit GAPs, and that the resulting high basal GTP levels mask the GTP-dependent increase in FRET efficiency of these probes.

Only in the probe pairs using PKN as the effector, the FRET efficiency of the Q63L mutant was markedly higher

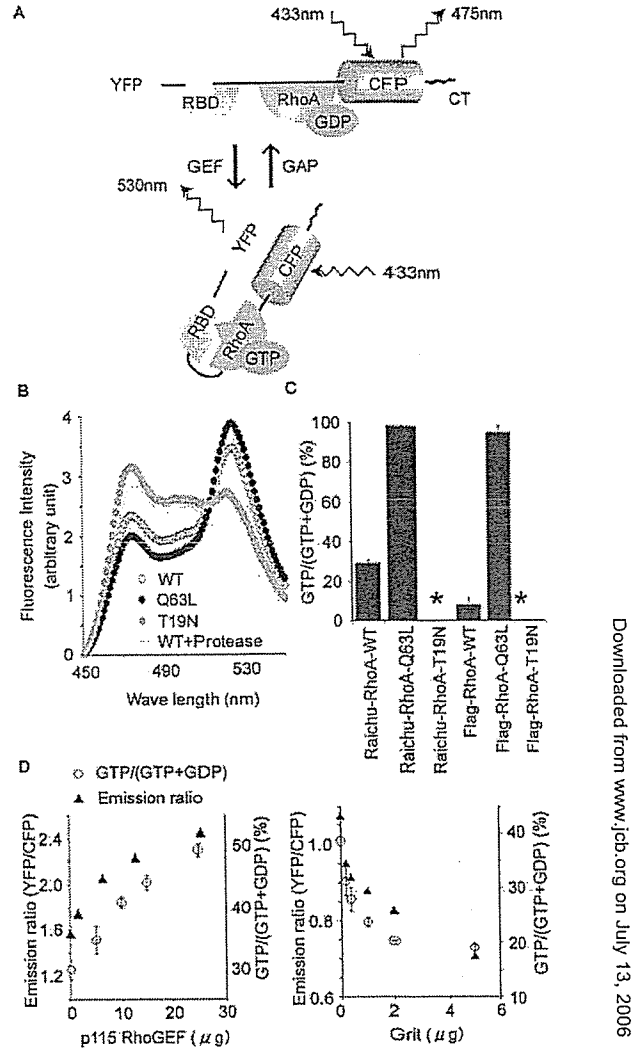

Figure 1. **Basic profile of Raichu-RhoA.** (A) Schematic representations of Raichu-RhoA bound to GDP or GTP. YFP and CFP denote a yellow- and cyan-emitting mutant of GFP, respectively. RBD indicates the RBD of the effector protein. (B) Emission spectra of Raichu-RhoA expressed in 293T cells at an excitation wavelength of 433 nm (left). WT, wild type; Q63L, GTPase-deficient mutant; T19N, a mutant with reduced affinity to guanine nucleotides. In the sample treated with protease, Raichu–RhoA–WT was cleaved with trypsin and proteinase K before analysis. (C) 293T cells expressing Raichu-RhoA and Flag-tagged RhoA were labeled with $^{32}P_i$. The guanine nucleotides bound to the GTPases were analyzed by TLC, and the average of two samples is shown with error bars. Asterisks indicate that the level of guanine nucleotides was beneath the detectable level. (D) pRaichu-RhoA was cotransfected into 293T cells with varying quantities of expression vectors for p115 RhoGEF and Grit. The emission ratio and GTP level were quantitated as in B and C. The emission intensities of CFP at 475 nm and YFP at 527 nm were used to calculate the emission ratio, YFP/CFP. Bars indicate error ranges. Experiments were repeated at least twice and representative data are shown.

than that of the wild-type probe (Table I). Because the gain was larger in the pair of Raichu–RhoA–1237X and –1238X, we characterized this set of probes further in the following analysis. As a negative control to Raichu–RhoA–1237X, we

Downloaded from www.jcb.org on July 13, 2006

Table I. Summary of the probes for RhoA activity

Plasmids[a] (WT/QL)	RhoA and effectors[b]		Emission ratio[c]			GTP
	NH_2 term	COOH term	WT	QL	Gain (%)[d]	WT (%)[e]
1202/1208	RhoA	mDia	1.15	1.12	−2.3	82 ± 0.1
1125/1126	RhoA	Rhotekin	1.47	1.49	1.4	73 ± 1.8
1206/1212	RhoA	Rhophilin	1.81	1.75	−3.2	86 ± 1.0
1240/1241	RhoA	PKN	1.48	1.72	15.7	22 ± 1.3
1214x/1220x	mDia	RhoA	1.22	1.31	8.0	72 ± 1.3
1104x/1105x	Rhotekin	RhoA	3.55	3.16	−11.3	76 ± 1.3
1218x/1224x	Rhophilin	RhoA	1.53	1.42	−7.4	80 ± 2.0
1237x/1238x	PKN	RhoA	1.57	2.09	32.7	33 ± 5.9
1110x/1111x	PAK	RhoA	1.0	0.9	−7.2	ND

[a]Numbers of Raichu probes are shown. WT, wild-type RhoA; QL, RhoA with the $Gln^{63}Leu$ mutation.
[b]The order of RhoA and the effectors from the NH_2 terminus to the COOH terminus are shown. For illustration, see Fig. 1.
[c]Probes were expressed in 293T cells and analyzed with a fluorescent spectrometer as described in the text. Emission intensities of YFP at 527 nm and CPF at 475 nm were used to calculate the emission ratio.
[d][(emission ratio of QL mutant) − (emission ratio of WT)]/(emission ratio of WT).
[e]Probes were expressed in 293T cells, labeled with $^{32}P_i$, and analyzed with TLC as described in the text. GTP/(GTP + GDP) is shown as a percentage.

generated Raichu–RhoA–1239X, in which Asn was substituted for Thr^{19} of RhoA to reduce the affinity to guanine nucleotides. As shown in Fig. 1 B, the FRET efficiency of Raichu–RhoA–1237X (WT) was between those of Raichu–RhoA–1238X (Q63L) and Raichu–RhoA–1239X (T19N). Occurrence of FRET was confirmed by treating cell lysates with trypsin and proteinase K as described previously (Mochizuki et al., 2001). The GTP ratio on Raichu–RhoA–1237X (WT) was 33%, whereas that on Flag–RhoA–WT was 8% (Fig. 1 C). The difference between Raichu–RhoA–1237X (WT) and Flag–RhoA–WT probably reflected the mild inhibition of GAP by the RBD of PKN. The GTP ratio on Raichu–RhoA–1238X (Q63L) and on Flag–RhoA–Q63L were 98 and 95%, respectively. In T19N mutants, binding of guanine nucleotides was not detectable as expected (Feig and Cooper, 1988). Because the FRET efficiency of Raichu–RhoA–1239X (T19N) was significantly lower than that of Raichu–RhoA–1237X (WT), the FRET efficiency of the nucleotide-free form must be lower than that of the GDP-bound form.

Correlation of FRET efficiency with GTP-loading

To further examine the correlation between GTP loading on Raichu–RhoA–1237X (WT) and the FRET efficiency, dose-responsive curves were obtained with cells expressing various quantities of p115 RhoGEF or Grit, a GAP for Rho-family GTPases (Nakamura et al., 2002). As shown in Fig. 1 D, both GTP loading and the emission ratio (YFP/CFP) increased by the expression of p115 RhoGEF and decreased by the expression of Grit, and both these effects were dose-dependent. These data demonstrated clearly that Raichu–RhoA–1237X (WT) was regulated by both GEFs and GAPs and validated its use in the monitoring of the balance between GEF and GAP activities for RhoA. Because the prototype Raichu–RhoA–1237X (WT) carries the carboxy-terminal region of Ki-Ras4B at its carboxy terminus, we call this probe Raichu–RhoA/K-Ras–CT hereafter. Also, we constructed a probe with the carboxy terminus of RhoA and named it Raichu–RhoA/RhoA–CT. We did not find any remarkable differences in the response to GEFs or GAPs between the two probes (unpublished data).

Development of Raichu-RBD

In addition to GEFs and GAPs, most Rho-family GTPases are regulated by another class of proteins, RhoGDI. To assess the activity of RhoGDI by monitoring the level of endogenous GTP-RhoA, we prepared another type of probe consisting of an RBD of effectors sandwiched by YFP and CFP (Fig. 2 A). We expected that the binding of endogenous GTP-RhoA to RBD in the probe displaced YFP and CFP, thereby decreasing the FRET efficiency. Again, we tested RBDs of mDia, Rhotekin, Rhophilin, and PKN for the optimization. We also tested several monomeric mutants of YFP and CFP (Zacharias et al., 2002) to improve the sensitivities of the probes. For the sake of simplicity, we will limit ourselves to a description of the best probe derived from the many trials, Raichu-1502 (hereafter used as Raichu-RBD), which consisted of monomeric YFP-$L^{222}K$/$F^{224}R$, the RBD of Rhotekin, and CFP. As shown in Fig. 2 B, the FRET efficiency of Raichu-RBD was decreased in the presence of wild-type RhoA or constitutively active RhoA, but not in the presence of dominant-negative RhoA, indicating that the decrease in FRET correlated with the binding to RhoA. Surprisingly, wild-type RhoA decreased FRET of the probe as efficiently as did the constitutively active RhoA. This may be explained by the property of Raichu-RBD that the FRET efficiency of Raichu-RBD–expressing cells correlated with the net amount of GTP-RhoA, but not with the GTP/GDP ratio on RhoA. In the overexpression system, the wild-type RhoA might provide a saturating amount of GTP-RhoA. Furthermore, we also examined the spectrogram of Raichu-RBD in living HeLa cells by using a flat field imaging spectrograph and obtained a similar result (Fig. 2 C). The difference in the emission ratio between Fig. 2 B and Fig. 2 C arose mostly from the difference in the filter sets used to dissect the fluorescences of YFP and CFP. These ob-

The Journal of Cell Biology

Downloaded from www.jcb.org on July 13, 2006

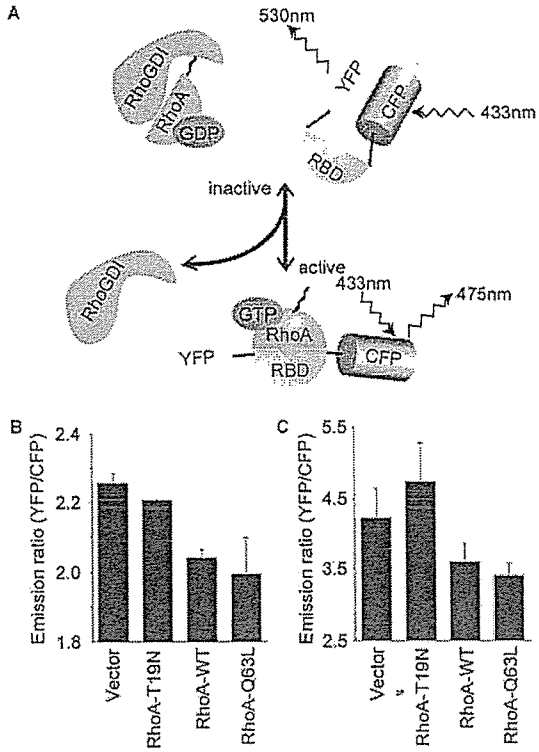

Figure 2. **Basic profile of Raichu-RBD.** (A) Schematic representations of Raichu-RBD unbound or bound to GTP-RhoA. RBD indicates the RBD of Rhotekin. (B) Cleared lysates of Raichu-RhoA–expressing 293T cells were used to obtain spectrograms at an excitation wavelength of 433 nm. The emission intensities of CFP at 475 nm and YFP at 527 nm were used to calculate the emission ratio, YFP/CFP (n = 3). Bars indicate SD. (C) Spectrograms of Raichu-RBD with or without Rho proteins were obtained in living HeLa cells. The emission intensities of CFP at 475 nm and YFP at 530 nm were used to calculate the emission ratio, YFP/CFP (n = 5). Bars indicate SD.

servations supported the idea that the FRET efficiency of Raichu-RBD reflected its binding to the endogenous RhoA. We also prepared a probe named Raichu–RBD–X, wherein carboxy terminus of RhoA was fused to Raichu-RBD. By placing the probe only to the membrane, we could reduce the background from the probe in the cytoplasm.

Imaging of the activities of Rho-family GTPases in living cells

Before FRET imaging, the intracellular localizations of the probes were compared with those of the Rho-family GTPases tagged with GFP (Fig. 3 A). The distribution of GFP-tagged Rho-family GTPases was in general agreement with the previous report (Michaelson et al., 2001); GFP–RhoA–WT was observed mostly in the cytoplasm, and GFP–Rac1–WT and GFP–Cdc42–WT were observed at both the plasma membrane and intracellular membrane compartments. The active forms of GFP-tagged Rho-family GTPases were detected both at the plasma membrane and the intracellular membrane compartments. The distribution of Raichu–RhoA/RhoA–CT, Raichu–Rac1/Rac1–CT, and Raichu–Cdc42/Cdc42–CT was indistinguishable from those of

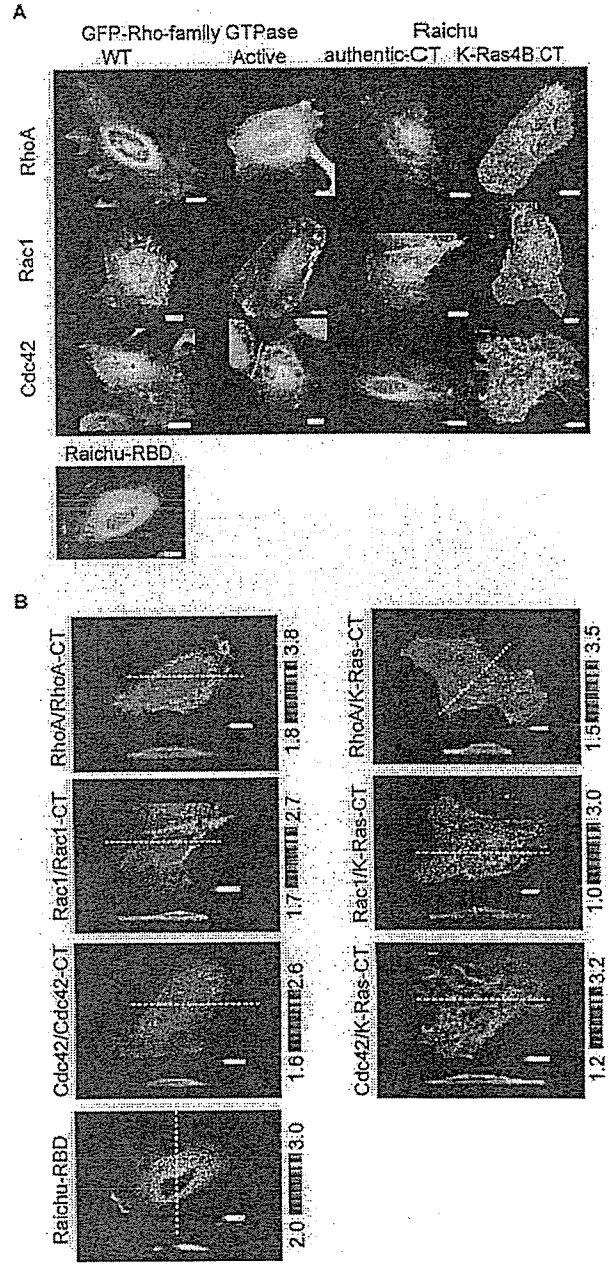

Figure 3. **Localization and FRET imaging of Raichu probes.** (A) HeLa cells expressing GFP-tagged Rho-family GTPases of the wild-type (WT) or constitutively active form (Active) are presented in the first two columns. The next two columns show HeLa cells expressing Raichu probes with either the authentic carboxy termini (CT) or K-Ras4B CT. A cell image of Raichu-RBD–expressing cells is also shown at the bottom of A. Cells were excited by an Argon laser at a 488-nm wavelength and imaged with a confocal microscope. (B) Ratio imaging by TPEM. HeLa cells expressing the Raichu probes listed on the left were imaged for YFP (535 ± 12 nm) and CFP (480 ± 15 nm) with a 790-nm excitation wavelength. XY planes from the bottom to the top of each cell were stacked, and the YFP/CFP ratio image is used to show the FRET efficiency in the intensity-modulated display mode. XZ sections were prepared along the dotted white lines. White bars indicate 10 μm (A and B). The upper and lower limits of the ratio range are shown at the right of each panel.

The Journal of Cell Biology

Downloaded from www.jcb.org on July 13, 2006

the constitutively active mutants, supporting the previous finding that the carboxy-terminal region primarily determines the localization of the Rho-family GTPases in their active forms (Michaelson et al., 2001; Fig. 3 A, third column). In a clear contrast, all probes with the carboxy terminus of K-Ras4B were localized mainly at the plasma membrane (Fig. 3 A, fourth column). The distribution of Raichu-RBD was typical for a cytosolic protein (Fig. 3 A, bottom).

Using these Raichu probes and two-photon excitation fluorescence microscopy (TPEM), which enabled us to minimize photobleaching during z-axis scanning and to increase signal-to-noise ratio, the activities of Rho-family GTPases were imaged in HeLa cells (Fan et al., 1999). Cells expressing Raichu probes were imaged for YFP (535 ± 12 nm) and CFP (480 ± 15 nm) with an excitation wavelength of 790 nm (Fig. 3 B). The YFP/CFP ratio image is used to show the FRET efficiency in the intensity-modulated display mode. A high FRET ratio of Raichu–RhoA/RhoA–CT was observed mostly at the plasma membrane. Very similar results were also obtained by using Raichu–Rac1/Rac1–CT and Raichu–Cdc42/Cdc42–CT. Thus, we concluded that the GEF/GAP balances of RhoA, Rac1, and Cdc42 were higher at the plasma membrane than at the intracellular membrane com-

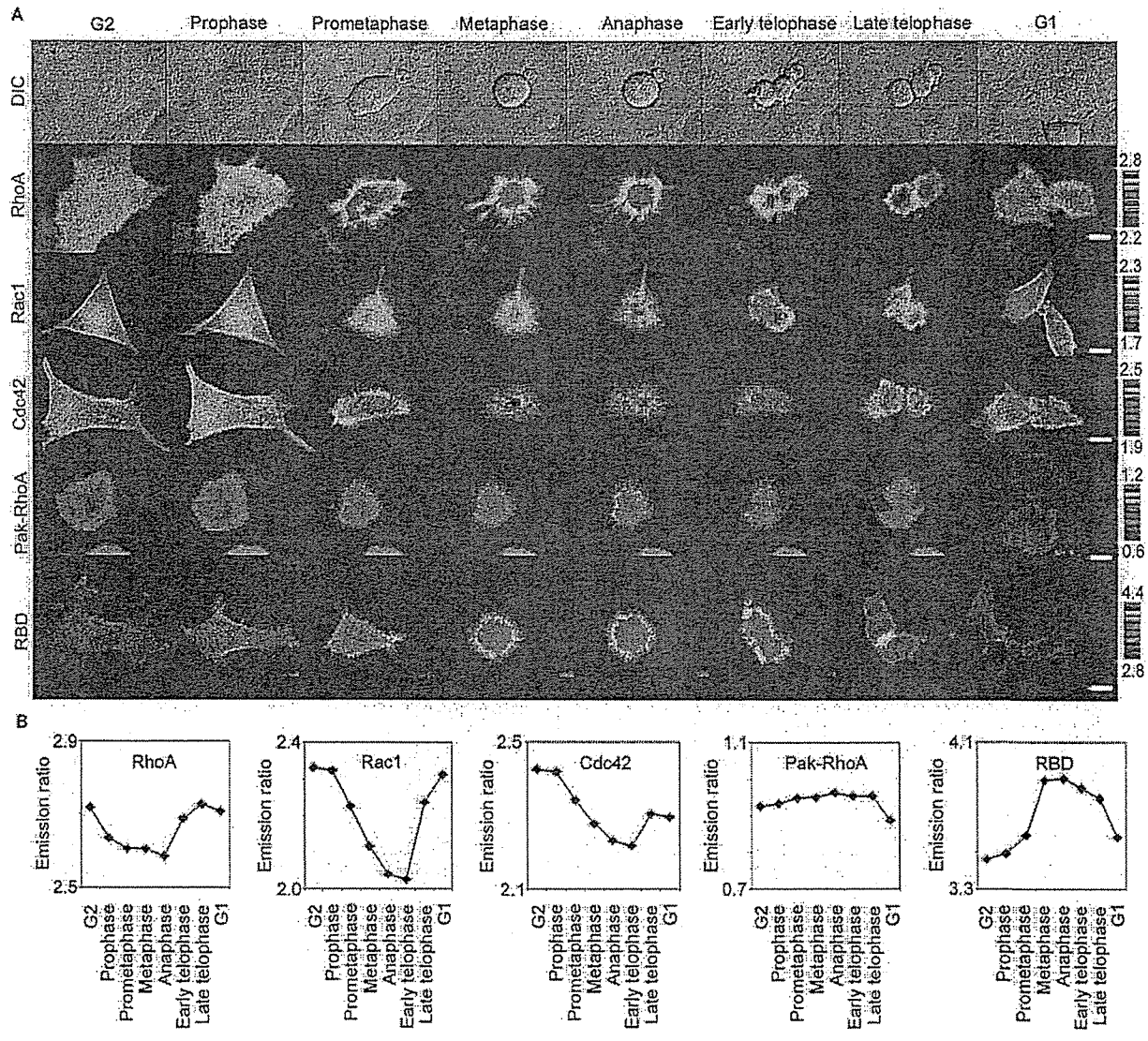

Figure 4. **Activities of Rho-family GTPases in HeLa cells progressing from G2 to G1 phase.** (A) HeLa cells were infected with recombinant adenoviruses for the expression of Raichu–RhoA/K-Ras–CT, Raichu–Rac1/K-Ras–CT, and Raichu–Cdc42/K-Ras–CT as indicated at left. Raichu–Pak–Rho and Raichu–RBD–X was introduced by lipofection. CFP, YFP, and differential interference contrast images were obtained every 2 min with a time-lapse epifluorescent microscope. A ratio image of YFP/CFP was used to represent FRET efficiency. The stages of cell cycle were determined by the differential interference contrast images. Representative FRET images are shown at each stage of the cell cycle denoted at the top of the figure. The upper and lower limits of the ratio range are shown at the right of each panel. At least six similar images were obtained for each probe, and a representative one is used here. White bars indicate 10 μm. (B) From the images in A, the net intensities of YFP and CFP in each cell were measured to calculate the averaged emission ratio.

The Journal of Cell Biology

Downloaded from www.jcb.org on July 13, 2006

partments in the interphase. Essentially the same conclusion was obtained by using the Raichu-RBD probe. Notably, binding of Raichu-RBD to the endogenous Rho decreases FRET efficiency (Fig. 2); therefore, in contrast to the other probes, the low FRET efficiency at the plasma membrane indicates a high level of GTP-Rho in this area. These observations are in agreement with the previous finding that RhoA, Rac, and Cdc42 are predominantly translocated to the plasma membrane by the expression of GEF or integrin stimulation (Etienne-Manneville and Hall, 2001; Michaelson et al., 2001; del Pozo et al., 2002). It should be emphasized that the presence of FRET probes at the intracellular membrane compartments hinders the detection of activity change at the plasma membrane when we use a conventional epifluorescence microscope. This is because we cannot eliminate signals from the intracellular membrane compartments without the use of a two-photon excitation microscope or a confocal microscope. Therefore, the Raichu probes with a K-Ras4B carboxy-terminal region, which were localized mostly at the plasma membrane (Fig. 3 B), were superior to the Raichu probes with the authentic carboxy termini in terms of the sensitivity in detecting the activity change at the plasma membrane. Hence, in many of the following experiments, we used Raichu–RhoA/K-Ras–CT because most of the activity change during cytokinesis was observed at the plasma membrane by TPEM. The occurrence of FRET in the cells was also confirmed by the previously reported photobleaching experiments (Miyawaki and Tsien, 2000); The FRET efficiencies were calculated as 29 ± 4.7% for Raichu–RhoA/K-Ras–CT and 46 ± 1.5% for Raichu-RBD.

Next, we tested if Raichu-RhoA could monitor the activity change of RhoA in the conditions where RhoA is known to be activated or inactivated. First, we observed diffuse increase in FRET efficiency in N1E-115 neuroblastoma cells expressing Raichu-RhoA and stimulated with lysophosphatidic acid (Fig. S1, available at http://www.jcb.org/cgi/content/full/jcb.200212049/DC1; Moolenaar, 1995). Second, nocodazole treatment of HeLa cells expressing Raichu–RhoA/K-Ras–CT increased in FRET efficiency (Fig. S1; Maddox and Burridge, 2003). Third, when cells expressing Raichu–RhoA/K-Ras–CT were treated with a RhoA inhibitor C3, FRET efficiency decreased (Fig. S2). In these experiments, the change in FRET efficiency correlated very well with the change in the level of endogenous GTP-RhoA as examined by the pull-down analysis.

Furthermore, to evaluate the effect of expression of Raichu-RhoA on the endogenous RhoA signaling cascade, we examined actin stress fiber formation (Fig. S3). We could

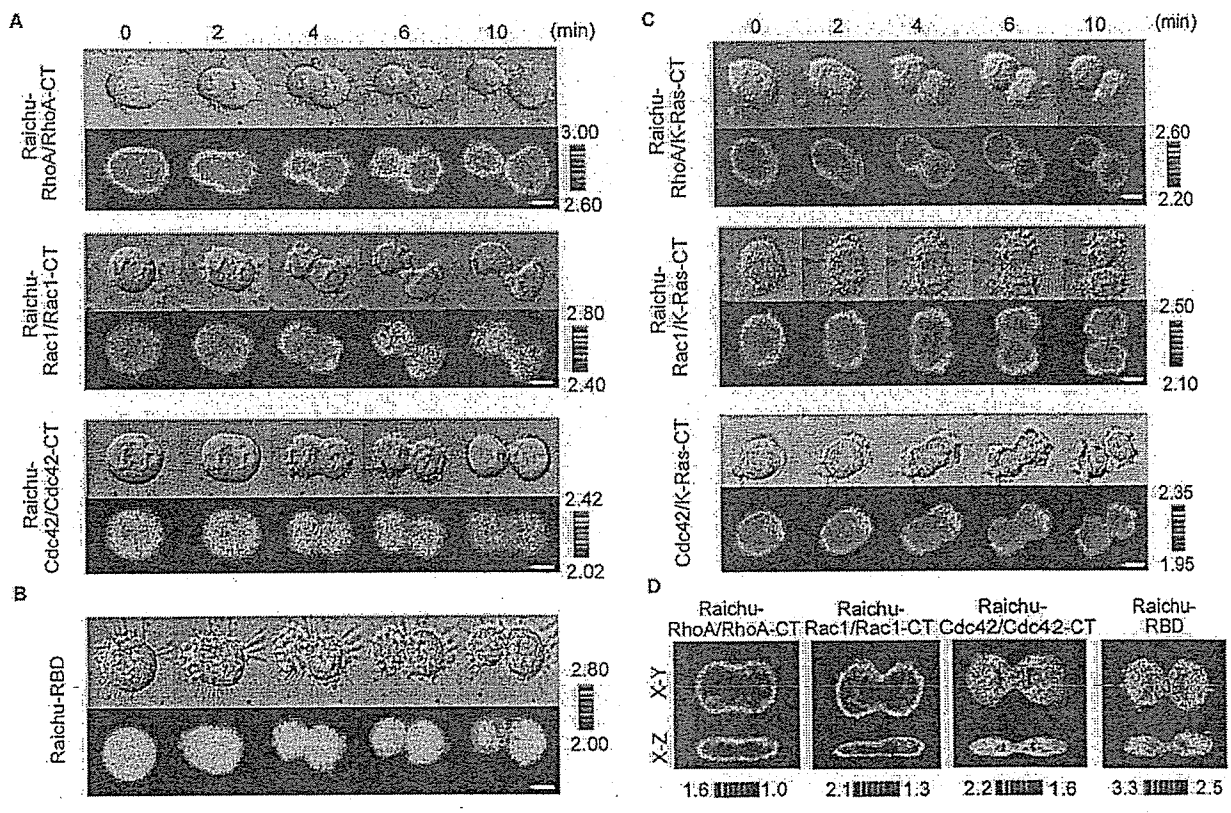

Figure 5. **Activity of Rho-family GTPases during cytokinesis.** HeLa cells expressing Raichu probes with carboxy termini of the authentic proteins (A) or Ki-Ras4B (C) or expressing Raichu-RBD (B) were photographed as in Fig. 4 A, except that the fluorescent images were focused at the middle depth of the cells and subjected to median filtering to reduce noise. The elapsed time is denoted at the top of the figure. The time zero is set to metaphase. At least six similar images were obtained for each probe, and a representative one is shown here. White bars indicate 10 μm. (D) HeLa cells expressing Raichu probes were imaged at early telophase by TPEM as in Fig. 3 B. Horizontal (X-Y) and vertical (X-Z) sections are shown.

The Journal of Cell Biology

Downloaded from www.jcb.org on July 13, 2006

not detect any difference in the formation of actin stress fiber between the nontransfected and transfected cells (Fig. S3), indicating that the expression of Raichu-RhoA did not perturb the RhoA signaling to a detectable level. Similarly, we could not detect any anomaly in cell shape, migration, or division by a modest expression of the probes.

Activity of Rho-family GTPases in HeLa cells progressing from G2 to G1 phase

Using these Raichu probes, we examined the activity of RhoA, Rac1, and Cdc42 in living HeLa cells progressing from G2 to G1 phase (Fig. 4 A; Videos 1–3). In this experiment, the objective lens was focused on the basal plasma membrane before imaging, and was fixed during the experiment. For this and the aforementioned reasons, we show here the results obtained by using the probes with K-Ras4B carboxy-terminal region, although we obtained essentially the same results with probes with the authentic carboxy-terminal regions. To show the time course of activity change more quantitatively, we calculated the emission ratios from the averaged intensities of YFP and CFP and plotted them against the cell cycle stage (Fig. 4 B). On entry into prophase, the level of RhoA activity decreased rapidly, leaving high activity at the periphery of the cells. After reaching its nadir at anaphase, the RhoA activity increased gradually in telophase. Essentially the same result was obtained by using Raichu-RhoA and Raichu-RBD. The activity of Rac1 decreased on the entry into prometaphase and reached its lowest level at early telophase, later than RhoA. After the midbody formation, Rac1 activity increased rapidly in the late telophase. Cdc42 activity changed essentially as did Rac1 activity, although the level of activity change was less remarkable. When we used Raichu–Cdc42/Cdc42–CT, we sometimes observed transient and moderate increase in Cdc42 activity in anaphase; however, we could not appreciate its significance at this moment. No detectable change in the FRET efficiency was observed in Raichu–Pak–Rho-expressing cells. We have obtained at least six similar video images of cell division for each probe.

Activity change of Rho-family GTPases during cytokinesis

Because the most drastic activity changes occurred after metaphase, we concentrated our efforts on the period from anaphase to telophase and performed experiments by continuously focusing at the middle depth of the cells (Fig. 5). In early telophase, the RhoA activity gradually increased at the plasma membrane, including the cleavage furrow. This increase was less pronounced when we used Raichu–RhoA/RhoA–CT (Fig. 5 A), but was more clear by using Raichu–RhoA/K-Ras4B–CT (Fig. 5 C) or by TPEM (Fig. 5 D). The increase in RhoA activity at the plasma membrane was confirmed by using Raichu-RBD (Fig. 5 B). In contrast to RhoA, the activity of Rac1 was suppressed at the center and started increasing from the polar sides of the plasma membrane at late telophase after the abscission of daughter cells (Fig. 5, A and C). Suppression of Rac1 activity at the cleavage furrow was more clearly depicted by TPEM (Fig. 5 D). The activity of Cdc42 was high at the intracellular membrane compartments and did not change remarkably from anaphase to telophase; however, we noticed that the activity always reached its nadir at the time of abscission of daughter cells (Fig. 5 A).

To examine if the activity change correlated with the accumulation of the Rho-family GTPases, localizations of GFP-tagged RhoA, Rac1, and Cdc42 were determined with a confocal microscope (Fig. S4). GFP-RhoA localized mostly in the cytoplasm, GFP-Rac1 both at the plasma membrane and cytoplasm, and GFP-Cdc42 at the intracellular membrane compartments. However, against our expectation, we did not observe remarkable change in the distribution of RhoA, Rac1, or Cdc42 during cytokinesis. RhoGDI may not contribute to the regulation of Rho-family GTPases during cytokinesis to a detectable level.

Discussion

It has been well documented that Rho-family GTPases are required for cytokinesis of many cell types (Prokopenko et al., 2000). Because stress fibers and focal contacts disassemble during cell division, it is predicted that Rho is deactivated as cells enter mitosis and is reactivated during cytokinesis (O'Connell et al., 1999). However, to the best of our knowledge, only two papers have examined Rho activity in relation to cell division (Kimura et al., 2000; Maddox and Burridge, 2003). Both groups have analyzed the level of GTP-RhoA by Bos' pull-down method in HeLa cells arrested at metaphase with nocodazole or taxol; however, the results are significantly different. Kimura et al. (2000) claim that RhoA activity remains low in G1 to S phase and increases remarkably at telophase. In contrast, Maddox and Burridge (2003) propose that RhoA activity increases at metaphase. Our observations agreed with Kimura's report (Kimura et al., 2000) in that RhoA activity started increasing after metaphase in HeLa cells, but disagreed with both reports in that the significant decrease in RhoA activity was found at the G2/M transition in our work. The discrepancy between the previous papers and ours may have arisen from the procedure to collect the mitotic cells before the pull-down analysis. On the other hand, we focused on the bottom of the cells during mitosis; therefore, on entry into M phase, the net intensities of both YFP and CFP were decreased by the rounding of the cells. It is possible that the observed activity change may be biased to the plasma membrane of the bottom of the cells.

It has been hypothesized that RhoA is specifically activated at the cleavage furrow during cytokinesis. The most supportive evidence for this hypothesis is that RhoA is recruited to the cleavage furrow in Swiss3T3 cells and sea urchin eggs (Takaishi et al., 1995; Nishimura et al., 1998). Further support comes from the findings that three Rho effectors, ROCK (Yasui et al., 1998; Kosako et al., 1999), mDia (Castrillon and Wasserman, 1994; Watanabe et al., 1997), and citron (Madaule et al., 1998) are recruited to the cleavage furrow. However, analyses using adherent cells have challenged this hypothesis, proposing that cytokinesis can take place through an "attachment-assisted mitotic cleavage" mechanism (Neujahr et al., 1997; Spudich, 1989; O'Connell et al., 1999). In this model, the decrease in RhoA activ-

The Journal of Cell Biology

Downloaded from www.jcb.org on July 13, 2006

The Journal of Cell Biology

ity causes cortical disintegration and cytokinesis in adherent cells (O'Connell et al., 1999). We support this model based on the following observations from the present work. First, RhoA activity decreased on entry into mitosis. Second, RhoA activity was not particularly concentrated at the cleavage furrow. Lastly, we barely detected an increase in RhoA activity at the plasma membrane of Rat1A cells before abscission of the daughter cells (unpublished data). Of note, we confirmed that GFP-citron was condensed at the cleavage furrow in HeLa cells (unpublished data). Thus, citron, and possibly other RhoA effectors involved in cytokinesis, may be accumulated at the cleavage furrow with the help of other unknown mechanisms.

Previous papers have shown that Rac and Cdc42 are involved in the cytokinesis of mammalian cells, based on the appearance of multinucleated cells in cells expressing constitutively active Rac1 or Cdc42 (Dutartre et al., 1996; Muris et al., 2002). Our observation that the activity of Rac1 and Cdc42 decreased during cytokinesis agrees with these previous reports and also with the finding that MgcRacGAP, a Rac GAP, accumulates at the mitotic spindle and midbody during cell division (Hirose et al., 2001). This suppression of Rac1 and Cdc42 may play a role in cytokinesis via Pak, an effector of Rac1 and Cdc42; Pak negatively regulates myosin light chain kinase, which phosphorylates and activates myosin II to induce actomyosin-based contraction (Sanders et al., 1999). Thus, suppression of Rac1 and Cdc42 may eventually promote constriction of actomyosin at the cleavage furrow.

After the construction of several trial probes, it has become clear that the affinity of the effector to GTPases should be moderate in order to develop a Raichu-RhoA probe with a wide dynamic range. Among the four effector proteins tested, only PKN yielded a probe that could be used for cell imaging. The GTP ratio on the probes with the effectors other than PKN were nearly (or greater than) 80%, indicating that these probes were refractory to GAPs. Because the GTP level on these probes did not significantly change by the orientation of effectors and RhoA, the linker regions used in Raichu probes seem to allow the effectors to fit flexibly into RhoA. For the same reason, it is also unlikely that steric confinement reduced the intrinsic GTPase activity of RhoA in these probes. Thus, we conclude that the high GTP levels on the probes reflect the high affinity of the effectors to RhoA. We observed a similar decrease in GAP sensitivity during the development of Raichu-Rap1 (Mochizuki et al., 2001). We originally constructed the Raichu-Rap1 probe with the Rap1-binding domain of RalGDS. In this probe, the GTP ratio on Raichu-Rap1 was >60%, whereas that on Flag-Rap1 was <5% in 293T cells (unpublished data). Only by replacing RalGDS with Raf was the GTP level on Raichu-Rap1 reduced to <25%. Notably, the affinity of Rap1 to RalGDS is remarkably higher than that to Raf (Herrmann et al., 1996). Thus, in order to develop probes for low mol wt GTPases, it is essential to search for a target molecule that possesses moderate affinity to the GTPases in order to minimize the inhibitory effect on GAP. Alternatively, we could introduce mutation into the effector-binding region of RhoA or the RhoA-binding region of the effector to reduce the affinity.

The finding that the GTP ratio on Raichu-RhoA was higher than that on the authentic RhoA may raise a question about the extent to which this probe reflects the activity change of GAPs. Because some GAPs prefer prenylated RhoA as their substrate (Molnar et al., 2001), intervention of CFP between RhoA and the prenylation signal at the carboxyl terminus may decrease the sensitivity of Raichu-RhoA to such GAPs. This problem is not limited to GAPs or prenylation. We cannot exclude the possibility that some Rho GEFs or Rho GAPs may not recognize Raichu-RhoA. In this regard, use of Raichu-RBD, which works on a different mechanism, will help to confirm the observation obtained by Raichu-RhoA.

In conclusion, we have shown the spatio-temporal regulation of Rho-family GTPases during cell division by two types of Raichu probes. One is able to monitor the local balance between GEFs and GAPs, and the other is able to depict the presence of GTP-Rho, enabling us to assess the contribution of all three regulators of Rho-family GTPases. Because none of the other existing methods can obtain spatio-temporal information on the activities of Rho-family GTPases in living cells, these Raichu probes will provide a versatile tool for exploring the role of these proteins in many research fields.

Materials and methods

Plasmids

pRaichu-Ras, pRaichu-Rac1, and pRaichu-Cdc42 have been described previously (Mochizuki et al., 2001; Itoh et al., 2002). Because the prototype Raichu-Rac1 and Raichu-Cdc42 are fused to the carboxy-terminal region of Ki-Ras4B, we call these Raichu–Rac1/K-Ras–CT and Raichu–Cdc42/K-Ras–CT, respectively. Raichu–Rac1/Rac1–CT and Raichu–Cdc42/Cdc42–CT were fused to the carboxy-terminal region of Rac1 (aa 172–192) and Cdc42 (aa 171–191), respectively. cDNA of Rhotekin was PCR amplified from a mouse spleen cDNA library (CLONTECH Laboratories, Inc.). cDNAs of mDia and Rhophilin were provided by S. Narumiya (Kyoto University, Kyoto, Japan). cDNA of PKN was obtained from Y. Ono (Kobe University, Kobe, Japan). An expression vector of p115 RhoGEF was obtained from T. Kozasa (University of Illinois, Chicago, IL). pCI-GritCD has been described previously (Nakamura et al., 2002). The coding region of human RhoA was subcloned into two eukaryotic expression vectors, pCXN2-Flag (Niwa et al., 1991) and pCAGGS-EGFP, to generate pCXN2–Flag–RhoA and pCAGGS–EGFP–RhoA, respectively.

Construction of Raichu probes for RhoA activity

cDNAs of the RBDs of effector proteins, including human mDia1 (aa 1–176), mouse Rhotekin (aa 1–88), mouse Rhophilin (aa 37–107), human PKN (aa 13–98), and a cDNA of the Rac1/Cdc42-binding domain of PAK (aa 68–150) were PCR amplified with primers carrying restriction enzyme recognition sites at their 5′ end, and subcloned into pCR®-Blunt II-TOPO® (Invitrogen). Plasmids for RhoA monitors were constructed using essentially the same procedure as was used to construct pRaichu-Ras (Mochizuki et al., 2001). From the amino terminus, Raichu–RhoA–1202, –1208, –1125, –1126, –1206, and –1212 consisted of YFP (aa 1–228), a spacer (Leu-Asp), wild-type or mutants of human RhoA (aa 1–189), a spacer (Thr-Gly-Gly-Gly-Gly-Thr), the RBD of effector proteins, a spacer (Gly-Gly-Arg), and CFP (aa 1–237). Raichu-1110X, -1111X, -1214X, -1220X, -1104X, -1105X, -1218X, and -1224X consisted of YFP (aa 1–228), a spacer (Leu-Asp), the RBD of effector proteins, a spacer (Thr-Gly-Gly-Gly-Gly-Thr), human RhoA (aa 1–189), a spacer (Gly-Gly-Arg), CFP (aa 1–237), a spacer (Ser-Arg), and the carboxy-terminal region of Ki-Ras4B (aa 169–188). Raichu–RhoA–1237X, –1238X, and –1239X consisted of YFP (aa 1–228), a spacer (Leu-Asp), the RBD of PKN, a spacer (Thr-Gly-Gly-Gly-Thr-Gly-Gly-Gly-Gly-Thr), wild-type or mutants of human RhoA (aa 1–189), a spacer (Gly-Gly-Arg), CFP (aa 1–237), a spacer (Gly-Arg-Ser-Arg), and the CAAX box of Ki-Ras4B (aa 169–188; Fig. 1 A). In Raichu–RhoA/RhoA–CT, the carboxy-terminal region of RhoA (aa 173–193) was substituted for that of Ki-Ras4B in Raichu–RhoA–1237X.

Downloaded from www.jcb.org on July 13, 2006

The Journal of Cell Biology

The effector proteins used in each probe are listed in Table I. In Raichu–RhoA–1239X, Asn was substituted for Thr[19] of RhoA. In the other probes, RhoA was either the wild-type or Gln[63]Leu mutant (Q63L), as denoted in Table I. In this paper, unless indicated otherwise, we used modified YFP [Thr[66]Gly, Val[69]Leu, Ser[73]Ala, Met[154]Thr, Val[164]Ala, Ser[176]Gly, and Thr[204]Tyr] and CFP [Lys[27]Arg, Tyr[67]Trp, Asp[130]Gly, Asn[147]Iso, Met[154]Thr, Val[164]Ala, Asn[165]His, Ser[176]Gly] as the acceptor and the donor, respectively. The nucleotide sequence of the coding regions of pRaichu–RhoA–1237X, which was used as a Raichu–RhoA/K-Ras–CT in this report, was deposited in the GenBank/EMBL/DDBJ databank (under accession no. AB074297).

Raichu–1502/Raichu–RBD consisted of YFP (aa 1–228), a spacer (Leu-Glu), the RBD of Rhotekin (aa 1–88), a spacer (Gly-Gly-Arg), and CFP (aa 1–237). In Raichu–1502/Raichu–RBD, a monomeric Venus [Phe[47]Leu, Thr[66]Gly, Val[69]Leu, Ser[73]Ala, Met[154]Thr, Val[164]Ala, Ser[176]Gly; and Thr[204]Tyr, Leu[222]Lys, Phe[224]Arg] (Nagai et al., 2002; Zacharias et al., 2002) was used as a YFP. In Raichu–Raichu–RBD–X, the carboxy-terminal region of RhoA was fused to Raichu-RBD.

Adenovirus vectors

A recombinant adenovirus for the expression of Raichu-RhoA was prepared by using the Adeno-X expression system (CLONTECH Laboratories, Inc.). In brief, the coding region of pRaichu–RhoA–1237X was first subcloned into pShuttle. Then, the expression unit including the cDNA of Raichu-RhoA was transferred to pAdeno-X by restriction enzyme cleavage and ligation. Finally, the adenovirus was produced from 293 cells transfected with the recombinant pAdeno-X. Recombinant adenoviruses carrying Raichu-RhoA were designated as Adeno–Raichu–RhoA. Preparation of the other recombinant adenoviruses was as described elsewhere (Itoh et al., 2002). Adeno–GFP–C3 was a gift from H. Kurose (Kyusyu University, Fukuoka, Japan).

Cells

HEK293 and HeLa cells were purchased from the Human Science Research Resources Bank (Sennan-shi, Japan). 293T and Swiss 3T3 cells were a gift from B.J. Mayer (University of Connecticut, Storrs, CT) and S. Narumiya (Kyoto University, Kyoto, Japan), respectively. Cells were maintained in DME (Sigma-Aldrich) supplemented with 10% FBS. Before the cell imaging, the medium was changed to phenol red–free MEM (Nissui).

In vitro spectrofluorometry

pRaichu plasmids were transfected into 293T cells by the calcium phosphate coprecipitation method with or without various quantities of plasmids for p115 Rho GEF, Grit-CD, or RhoA as described previously (Mochizuki et al., 2001). 36 h later, cells were harvested in lysis buffer (20 mM Tris-HCl, pH 7.5, 100 mM NaCl, 0.5% Triton X-100, and 5 mM $MgCl_2$) and clarified by centrifugation. Fluorescence spectra were obtained with a fluorescent spectrometer (model FP-750; JASCO Co.) using an excitation wavelength of 433 nm. For the demonstration of FRET, the cell lysates were incubated with 12.5 μg/ml trypsin and 50 μg/ml proteinase K at 37°C for 10 min and analyzed with the spectrometer.

Imaging spectrofluorometry

Plasmids encoding Raichu probes were transfected into HeLa cells using SuperFect® (QIAGEN) with or without plasmids for RhoA wild-type or mutants. 36 h later, cells were imaged on an inverted microscope (model IX71; Olympus) that was equipped with a flat field imaging spectrograph (SpectraPro 150; Acton Research Co.), a cooled CCD camera (Spec-10: 256E; Roper Scientific), and WinSpec32 software (Roper Scientific). Cells were observed with a 75-W Xenon lamp with a 12% ND filter (Olympus), an excitation filter (MX0420; Asahi Spectra Co.), a dichroic mirror (445DRLP; Omega Optical Inc.), and an oil immersion objective lens (60× Plan Apo; Olympus).

Analysis of guanine nucleotides bound to GTPases

Guanine nucleotides bound to Raichu probes and Flag-RhoA were analyzed essentially as described previously (Gotoh et al., 1997). In brief, 293T cells were transfected with pRaichu-RhoA or pCXN2–Flag–RhoA. 36 h after transfection, cells were labeled with $^{32}P_i$ in phosphate-free modified Eagle's medium (Invitrogen) for 4 h. Raichu-RhoA and Flag-RhoA were immunoprecipitated with anti-GFP antibody prepared in the Matsuda laboratory and anti-Flag M2 mAb (Sigma-Aldrich), respectively. The immunoprecipitates were boiled and analyzed by TLC. The amount of GTP and GDP bound to RhoA was quantitated with an image analyzer (BAS-1000; Fuji Film).

Imaging of RhoA activity in living cells

HeLa cells transfected with pRaichu-derived vectors or infected with recombinant adenoviruses were imaged every 2 min on an inverted microscope (model IX70; Olympus) that was equipped with a cooled CCD camera (CoolSNAP HQ™; Roper Scientific), and controlled by MetaMorph® software (Universal Imaging Corp.; Miyawaki et al., 1997). For dual-emission ratio imaging of Raichu probes, we used a 440AF21 excitation filter, a 455DRLP dichroic mirror, and two emission filters; 480AF30 for CFP and 535AF26 for YFP (all filters and mirrors from Omega Optical, Inc.). Cells were illuminated with a 75-W Xenon lamp through a 12% ND filter (Olympus) and a 100× oil immersion objective lens. The exposure time was 0.5 s when the binning of the CCD camera was set to 4 × 4. After background subtraction, the ratio image of YFP/CFP was created with MetaMorph® software and used to represent FRET efficiency. For the photobleaching experiment, Raichu-RhoA–expressing cells were illuminated without an ND filter for 5 min. In this experiment, we used an excitation filter (MX510; Asahi Spectra Co.) and a dichroic mirror (XF2052; Omega Optical, Inc.). FRET efficiency was calculated by the following equation: FRET efficiency = 1 − (CFP prebleach/CFP postbleach).

Confocal microscopy and TPEM

Cells were observed with a multi-photon excitation microscope (model FV500; Olympus) equipped with external photomultiplier tubes, an Argon laser, an He:Ne laser, and a MAITAI Ti:sapphire laser (Spectra Physics). The MAITAI laser was capable of generating a >100-fs pulse at a repetition rate of 80 MHz. The output wavelength was tunable from 780 to 920 nm. The output laser beam, with a power >0.7 W, was horizontally polarized. The excitation wavelength for the TPEM was 790 nm as described previously (Fan et al., 1999). For the FRET imaging, we used an IR-cut filter (RDM650; Olympus), a dichroic mirror (DM505; Olympus), and two emission filters; 480AF30 for CFP and 535AF26 for YFP (Omega Optical, Inc.). For the conventional confocal imaging with the Argon laser, we used two dichroic mirrors, DM458/515 and SDM 515; and emission filters, BA480–495 for CFP and BA535–565 for YFP (Olympus).

Online supplemental material

Time-lapse FRET images of Fig. 4 are compiled into QuickTime videos available as supplemental material. Videos 1–3 show the cell division of HeLa cells expressing Raichu–RhoA/K-Ras–CT, Raichu–Rac1/K-Ras–CT, and Raichu–Cdc42/K-Ras–CT, respectively. Differential interference contrast, CFP, and YFP images were acquired every 2 min overnight, and frames spanning cell division were used to create video files. FRET images are shown in the IMD mode. The video is displayed at 15 frames/s. Fig. S1 to Fig. S4 show basic properties of Raichu probes. Online supplemental material available at http://www.jcb.org/cgi/content/full/jcb.200212049/DC1.

We thank N. Yoshida, N. Fujimoto, and Y. Matsuura for their technical assistance.

This work was supported in part by Special Coordination Funds for Promoting Science and Technology from the Ministry of Education, Science, Sports and Culture of Japan, and grants from the Health Science Foundation and Yasuda Medical Research Foundation, Japan (to M. Matsuda).

Submitted: 6 December 2002
Revised: 27 May 2003
Accepted: 29 May 2003

References

Bishop, A.L., and A. Hall. 2000. Rho GTPases and their effector proteins. *Biochem. J.* 348:241–255.

Castrillon, D.H., and S.A. Wasserman. 1994. Diaphanous is required for cytokinesis in *Drosophila* and shares domains of similarity with the products of the limb deformity gene. *Development.* 120:3367–3377.

del Pozo, M.A., W.B. Kiosses, N.B. Alderson, N. Meller, K.M. Hahn, and M.A. Schwartz. 2002. Integrins regulate GTP-Rac localized effector interactions through dissociation of Rho-GDI. *Nat. Cell Biol.* 4:232–239.

Drechsel, D.N., A.A. Hyman, A. Hall, and M. Glotzer. 1997. A requirement for Rho and Cdc42 during cytokinesis in *Xenopus* embryos. *Curr. Biol.* 7:12–23.

Dutartre, H., J. Davoust, J.P. Gorvel, and P. Chavrier. 1996. Cytokinesis arrest and redistribution of actin-cytoskeleton regulatory components in cells expressing the Rho GTPase CDC42Hs. *J. Cell Sci.* 109:367–377.

Etienne-Manneville, S., and A. Hall. 2001. Integrin-mediated activation of Cdc42

Downloaded from www.jcb.org on July 13, 2006

controls cell polarity in migrating astrocytes through PKCzeta. *Cell.* 106: 489–498.

Fan, G.Y., H. Fujisaki, A. Miyawaki, R.K. Tsay, R.Y. Tsien, and M.H. Ellisman. 1999. Video-rate scanning two-photon excitation fluorescence microscopy and ratio imaging with cameleons. *Biophys. J.* 76:2412–2420.

Feig, L.A., and G.M. Cooper. 1988. Inhibition of NIH3T3 cell proliferation by a mutant ras protein with preferential affinity for GDP. *Mol. Cell. Biol.* 8:3235–3243.

Gotoh, T., Y. Niino, M. Tokuda, O. Hatase, S. Nakamura, M. Matsuda, and S. Hattori. 1997. Activation of R-Ras by ras-guanine nucleotide-releasing factor. *J. Biol. Chem.* 272:18602–18607.

Heim, R., and R.Y. Tsien. 1996. Engineering green fluorescent protein for improved brightness, longer wavelengths and fluorescence resonance energy transfer. *Curr. Biol.* 6:178–182.

Herrmann, C., G. Horn, M. Spaargaren, and A. Wittinghofer. 1996. Differential interaction of the Ras family GTP-binding proteins H-Ras, Rap1A, and R-Ras with the putative effector molecules Raf kinase and Ral-guanine nucleotide exchange factor. *J. Biol. Chem.* 271:6794–6800.

Hirose, K., T. Kawashima, I. Iwamoto, T. Nosaka, and T. Kitamura. 2001. MgcRacGAP is involved in cytokinesis through associating with mitotic spindle and midbody. *J. Biol. Chem.* 276:5821–5828.

Itoh, R.E., K. Kurokawa, Y. Ohba, H. Yoshizaki, N. Mochizuki, and M. Matsuda. 2002. Activation of Rac and Cdc42 video-imaged by FRET-based single-molecule probes in the membrane of living cells. *Mol. Cell. Biol.* 22:6582–6591.

Kimura, K., T. Tsuji, Y. Takada, T. Miki, and S. Narumiya. 2000. Accumulation of GTP-bound RhoA during cytokinesis and a critical role of ECT2 in this accumulation. *J. Biol. Chem.* 275:17233–17236.

Kishi, K., T. Sasaki, S. Kuroda, T. Itoh, and Y. Takai. 1993. Regulation of cytoplasmic division of *Xenopus* embryo by rho p21 and its inhibitory GDP/GTP exchange protein (rho GDI). *J. Cell Biol.* 120:1187–1195.

Kosako, H., H. Goto, M. Yanagida, K. Matsuzawa, M. Fujita, Y. Tomono, T. Okigaki, H. Odai, K. Kaibuchi, and M. Inagaki. 1999. Specific accumulation of Rho-associated kinase at the cleavage furrow during cytokinesis: cleavage furrow-specific phosphorylation of intermediate filaments. *Oncogene.* 18:2783–2788.

Kosako, H., T. Yoshida, F. Matsumura, T. Ishizaki, S. Narumiya, and M. Inagaki. 2000. Rho-kinase/ROCK is involved in cytokinesis through the phosphorylation of myosin light chain and not ezrin/radixin/moesin proteins at the cleavage furrow. *Oncogene.* 19:6059–6064.

Kraynov, V.S., C. Chamberlain, G.M. Bokoch, M.A. Schwartz, S. Slabaugh, and K.M. Hahn. 2000. Localized rac activation dynamics visualized in living cells. *Science.* 290:333–337.

Mabuchi, I., Y. Hamaguchi, H. Fujimoto, N. Morii, M. Mishima, and S. Narumiya. 1993. A rho-like protein is involved in the organisation of the contractile ring in dividing sand dollar eggs. *Zygote.* 1:325–331.

Madaule, P., M. Eda, N. Watanabe, K. Fujisawa, T. Matsuoka, H. Bito, T. Ishizaki, and S. Narumiya. 1998. Role of citron kinase as a target of the small GTPase Rho in cytokinesis. *Nature.* 394:491–494.

Maddox, A.S., and K. Burridge. 2003. RhoA is required for cortical retraction and rigidity during mitotic cell rounding. *J. Cell Biol.* 160:255–265.

Michaelson, D., J. Silletti, G. Murphy, P. D'Eustachio, M. Rush, and M.R. Philips. 2001. Differential localization of Rho GTPases in live cells: regulation by hypervariable regions and RhoGDI binding. *J. Cell Biol.* 152:111–126.

Mitra, R.D., C.M. Silva, and D.C. Youvan. 1996. Fluorescence resonance energy transfer between blue-emitting and red-shifted excitation derivatives of the green fluorescent protein. *Gene.* 173:13–17.

Miyawaki, A., and R.Y. Tsien. 2000. Monitoring protein conformations and interactions by fluorescence resonance energy transfer. *Methods Enzymol.* 327: 472–500.

Miyawaki, A., J. Llopis, R. Heim, J.M. McCaffery, J.A. Adams, M. Ikura, and R.Y. Tsien. 1997. Fluorescent indicators for Ca^{2+} based on green fluorescent proteins and calmodulin. *Nature.* 388:882–887.

Mizuno, H., A. Sawano, P. Eli, H. Hama, and A. Miyawaki. 2001. Red fluorescent protein from *Discosoma* as a fusion tag and a partner for fluorescence resonance energy transfer. *Biochemistry.* 40:2502–2510.

Mochizuki, N., S. Yamashita, K. Kurokawa, Y. Ohba, T. Nagai, A. Miyawaki, and M. Matsuda. 2001. Spacio-temporal images of growth factor-induced activation of Ras and Rap1. *Nature.* 411:1065–1068.

Molnar, G., M.C. Dagher, M. Geiszt, J. Settleman, and E. Ligeti. 2001. Role of prenylation in the interaction of Rho-family small GTPases with GTPase activating proteins. *Biochemistry.* 40:10542–10549.

Moolenaar, W.H. 1995. Lysophosphatidic acid, a multifunctional phospholipid messenger. *J. Biol. Chem.* 270:12949–12952.

Muris, D., T. Verschoor, N. Divecha, and R. Michalides. 2002. Constitutive active GTPases Rac and Cdc42 are associated with endoreplication in PAE cells. *Eur. J. Cancer.* 38:1775–1782.

Nagai, T., K. Ibata, E.S. Park, M. Kubota, K. Mikoshiba, and A. Miyawaki. 2002. A variant of yellow fluorescent protein with fast and efficient maturation for cell-biological applications. *Nat. Biotechnol.* 20:87–90.

Nakamura, T., M. Komiya, K. Sone, E. Hirose, N. Gotoh, H. Morii, Y. Ohta, and N. Mori. 2002. Grit, a GTPase-activating protein for the Rho family, regulates neurite extension through its association with TrkA receptor and N-Shc, CrkL/Crk adapter molecules. *Mol. Cell. Biol.* 22:8721–8734.

Narumiya, S. 1996. The small GTPase Rho: cellular functions and signal transduction. *J. Biochem. (Tokyo).* 120:215–228.

Neujahr, R., C. Heizer, and G. Gerisch. 1997. Myosin II-independent processes in mitotic cells of *Dictyostelium discoideum*: redistribution of the nuclei, rearrangement of the actin system and formation of the cleavage furrow. *J. Cell Sci.* 110:123–137.

Nishimura, Y., K. Nakano, and I. Mabuchi. 1998. Localization of Rho GTPase in sea urchin eggs. *FEBS Lett.* 441:121–126.

Niwa, H., K. Yamamura, and J. Miyazaki. 1991. Efficient selection for high-expression transfectants with a novel eukaryotic vector. *Gene.* 108:193–200.

O'Connell, C.B., S.P. Wheatley, S. Ahmed, and Y.L. Wang. 1999. The small GTP-binding protein rho regulates cortical activities in cultured cells during division. *J. Cell Biol.* 144:305–313.

Olofsson, B. 1999. Rho guanine dissociation inhibitors: pivotal molecules in cellular signalling. *Cell. Signal.* 11:545–554.

Prokopenko, S.N., R. Saint, and H.J. Bellen. 2000. Untying the Gordian knot of cytokinesis. Role of small G proteins and their regulators. *J. Cell Biol.* 148: 843–848.

Sanders, L.C., F. Matsumura, G.M. Bokoch, and P. de Lanerolle. 1999. Inhibition of myosin light chain kinase by p21-activated kinase. *Science.* 283:2083–2085.

Spudich, J.A. 1989. In pursuit of myosin function. *Cell Regul.* 1:1–11.

Takai, Y., T. Sasaki, and T. Matozaki. 2001. Small GTP-binding proteins. *Physiol. Rev.* 81:153–208.

Takaishi, K., T. Sasaki, T. Kameyama, S. Tsukita, S. Tsukita, and Y. Takai. 1995. Translocation of activated Rho from the cytoplasm to membrane ruffling area, cell-cell adhesion sites and cleavage furrows. *Oncogene.* 11:39–48.

Watanabe, N., P. Madaule, T. Reid, T. Ishizaki, G. Watanabe, A. Kakizuka, Y. Saito, K. Nakao, B.M. Jockusch, and S. Narumiya. 1997. p140mDia, a mammalian homolog of *Drosophila* diaphanous, is a target protein for Rho small GTPase and is a ligand for profilin. *EMBO J.* 16:3044–3056.

Yasui, Y., M. Amano, K. Nagata, N. Inagaki, H. Nakamura, H. Saya, K. Kaibuchi, and M. Inagaki. 1998. Roles of Rho-associated kinase in cytokinesis; mutations in Rho-associated kinase phosphorylation sites impair cytokinetic segregation of glial filaments. *J. Cell Biol.* 143:1249–1258.

Zacharias, D.A., J.D. Violin, A.C. Newton, and R.Y. Tsien. 2002. Partitioning of lipid-modified monomeric GFPs into membrane microdomains of live cells. *Science.* 296:913–916.

Zhang, J., R.E. Campbell, A.Y. Ting, and R.Y. Tsien. 2002. Creating new fluorescent probes for cell biology. *Nat. Rev. Mol. Cell Biol.* 3:906–918.

The Journal of Cell Biology

Downloaded from www.jcb.org on July 13, 2006

総 合 論 文

核内受容体Peroxisome Proliferator-Activated Receptorを介する誘導型シクロオキシゲナーゼの発現調節に関する研究*

国立循環器病センター研究所薬理部**

井上 裕康

Vitamins (Japan), **77** (8), 449-458 (2003)

Studies on Regulation of Inducible Cyclooxygenase Expression by Nuclear Receptor PPAR

Hiroyasu INOUE

Department of Pharmacology, National Cardiovascular Center Research Institute, 5-7-1 Fujishiro-dai, Suita, Osaka 565-8565, Japan

Cyclooxygenase-2 (COX-2), a rate-limiting enzyme for prostaglandins (PG) synthesis, plays a key role in inflammation, tumorigenesis, development and circulatory homeostasis. The PGD_2 metabolite 15-deoxy-$\Delta^{12,14}PGJ_2$ (15d-PGJ_2) was identified as a potent natural ligand for the peroxisome proliferator-activated receptor-γ (PPARγ). 15d-PGJ_2 suppresses the lipopolysaccharide (LPS)-induced expression of COX-2 in the macrophage-like differentiated U937 cells, but not in vascular endothelial cells. PPARγ mRNA expressed abundantly in the U937 cells is down-regulated by LPS. In contrast, LPS up-regulates mRNA for the glucocorticoid receptor, and its ligand dexamethasone (DEX) strongly suppresses the LPS-induced expression of COX-2 gene. Transfection of a PPARγ-expression vector into the endothelial cells acquires this suppressive regulation of COX-2 gene transcription by 15d-PGJ_2, but not by DEX. Taken together, we propose that expression of COX-2 will be regulated by a negative feedback loop mediated through PPARγ, which makes possible a dynamic production of PG, especially in macrophages, and may attribute to various expression patterns and physiological functions of COX-2.

Key words : cyclooxygenase, PPAR, regulation, nuclear receptor, transcription

(*Received April 21, 2003*)

1. はじめに

シクロオキシゲナーゼ(COX)はプロスタグランジン(PG)産生の律速酵素で，必須脂肪酸であるアラキドン酸を基質にしてPGH_2を生成する反応を触媒する．非ステロイド性抗炎症薬の作用は，COX活性の阻害によるPG産生抑制を介している．COXには，構成型発現を示すCOX-1と誘導型COX-2の2種類のアイソザイムが見いだされている．COX-2の発現は炎症性刺激で迅速に誘導されること，抗炎症性ステロイド剤であるグ

*本論文は，日本ビタミン学会第54回大会(平成14.4.25～26,東京)における奨励賞受賞講演をまとめたものである．

**〒565-8565 吹田市藤白台5-7-1

ルココルチコイドによって著明に抑制されることから，炎症反応に深くかかわっている．最近開発されたCOX-2選択的阻害剤は，COX-1活性阻害に由来する副作用が少ない薬剤として注目されている．さらに，COX-2ノックアウトマウスの解析や最近の臨床を含む研究などから，COX-2が発がん，アルツハイマー病，循環器系疾患にも関与していることが示唆され，COX-2が炎症だけではなく生物学的および医学的に重要な役割を担っていることが次第に明らかになってきた[1)-5)]．

Peroxisome proliferator-activated receptor (PPAR) は核内受容体ファミリーに属するリガンド依存性転写因子で，そのファミリーの中にはグルココルチコイドのような脂溶性ホルモンや脂溶性ビタミンをリガンドとする受容体などが含まれる[6)]．PPARには，現在3種類のサブタイプα，γ，δ（またはβ）が知られている．PPARαは主に肝臓，腎臓に，PPARγは主に脂肪細胞，マクロファージに，PPARδは様々な組織に発現している．PPARαに対する合成リガンド・フィブレート系誘導体は高脂血症治療薬として，PPARγに対する合成リガンド・チアゾリジン系誘導体はインスリン抵抗性改善薬として知られており，PPARは生活習慣病改善薬の標的分子として現在注目を集めている[7)]．PPARγの内因性リガンドはいまだ不明であるが，その候補としてPGD2の代謝産物15-deoxy-$\Delta^{12,14}$ PGJ2（15d-PGJ2）が報告された[8)9)]．また，アラキドン酸をはじめとする必須脂肪酸やその代謝産物，非ステロイド性抗炎症薬などもPPARのリガンドとして働く可能性が指摘され，食生活とも密接にかかわる核内受容体であることが分かってきた（図1）[7)10)]．さらにPPARが関与していると考えられる生体内での役割は，前述したCOX-2が関与する役割と重複している部分が多い（表1）．したがって，COX経路とPPARの相互作用はそれぞれの生理的役割や薬剤の作用機構を理解する上で，重要な研究対象と考えられる．本稿では，マクロファージ系細胞におけるCOX-2発現のPPARγによるフィードバック制御機構を概説するとともに，今後の展望について議論したい．

2. 細胞の種類によって異なるCOX-2の発現調節

循環器系においては，プロスタサイクリン（PGI2）と

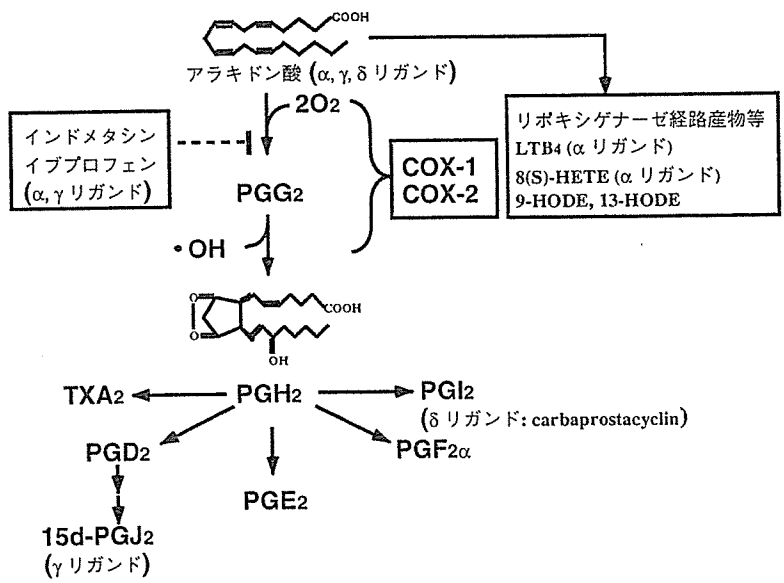

図1．シクロオキシゲナーゼ経路とPPARリガンド．
プロスタグランジン産生系などアラキドン酸代謝物，およびその阻害剤の中に，PPARのリガンドとして働くものがいくつか報告されている．ただし，これらはPPARに対する結合能で検出され，高濃度でのみ働くものも多い．したがって，これらが実際に生体内でPPARを介して機能しているかどうかはさらに検討を要する．最近，血清中に存在する脂質性増殖因子の主要成分・リゾホスファチジン酸が細胞内でPPARγアゴニストとして働くことが報告された[11)]．
図脚注
LTB4: leukotriene（ロイコトリエン）B4
HETE: hydroxyeicosatetraenoic acid（ヒドロキシエイコサテトラエン酸）
HODE: hydroxyoctadecadienoic acid（ヒドロキシオクタデカジエン酸）

表1．COX-2とPPARの関連性．

	COX-2	PPAR
炎症反応	非ステロイド性抗炎症薬(NSAIDs)の薬効とCOX活性阻害によるPG産生抑制の相関[1)-5)]	PPARγリガンドによる炎症性サイトカイン産生抑制[12)]
発がん	新しい抗腫瘍剤候補としてのCOX-2選択的阻害剤[13)]	PPARγリガンドのがんに対する種々の効果[14)-16)]
初期発生	COX-2ノックアウトマウス雌における初期発生異常[17)]	COX-2由来PGI2のPPARδを介する初期胚着床への関与[18)]
インスリン分泌調節	IL-1βによるグルコース依存性インスリン分泌抑制におけるCOX-2由来PGE2の関与[19)]	PPARγ合成リガンドによるインスリン抵抗性の改善[7)]

それに拮抗する作用を持つトロンボキサン(TXA2)の産生のバランスがホメオスターシスに重要であり，そのバランスの破綻は動脈硬化症をはじめとする様々な病態と関連している．PGI2は主に血管内皮細胞で，TXA2は血小板や活性化マクロファージで産生されるが，血小板以外の細胞ではCOX-2の発現が種々の刺激により誘導され，それぞれのPG類産生に寄与している．我々はその視点から，PGI2を産生する血管内皮細胞とTXA2，PGE2を産生するマクロファージ系U937細胞でのCOX-2発現の相違に注目して研究を進めている[20)-26)]．さらに，がん細胞をはじめとする種々の細胞におけるCOX-2の発現調節について共同研究を進めてきた[27)-40)]．その結果，COX-2遺伝子のプロモーター領域に存在する転写因子結合配列のうち，cAMP応答エレメント(CRE)，nuclear factor-interleukin 6(NF-IL6)およびnuclear factor-κB(NF-κB)結合配列がCOX-2の転写調節に関与していること，これらのシスエレメントに種々の転写因子が細胞種，刺激剤，時間等の相違により異なった組み合わせで作用することを明らかにしてきた．図2に，マクロファージ系細胞と血管内皮細胞でのCOX-2遺伝子の異なった発現機構についてまとめた．以下にそれらについて記述する．

2-1．マクロファージ系U937細胞

マクロファージ様に分化したU937細胞を，エンドトキシンであるリポポリサッカライド(LPS)で刺激するとTXA2の産生が認められる[41)]が，これは活性化した腹腔マクロファージにおけるCOX-2およびトロンボキサン合成酵素mRNAの発現パターンとほぼ一致している[22)]．LPSによるCOX-2mRNAの誘導は，刺激後30分で観察された．ヒトCOX-2遺伝子の変異プロモーター(327/+59)で転写制御されるルシフェラーゼレポーターベクターを安定導入したU937細胞の解析から，プロモーター領域のNF-κB結合配列がLPSによる誘導に関与することが示唆された[23)]．この時NF-κBが活性化されるが，その活性化は細胞質中において複合体を形成している阻害剤κB分解による核への移行であり，新たなタンパク質合成を必要としない．なお，NF-κB結合配列が働くためにはその前提条件としてU937細胞が増殖をとめ，マクロファージ様に分化していることが必要であり，そのためにはCREに結合する転写因子が重要であることが示唆された[20)]．

2-2．血管内皮細胞

ウシ頸動脈由来内皮細胞(BAEC)をLPS刺激すると，COX-2mRNAの発現が1時間程の時間差を持って誘導される．このCOX-2の発現パターンは，既述した迅速で顕著な誘導であるU937細胞とは異なっていた[21)]．BAECにおけるCOX-2の転写調節について，1) CRE，NF-IL6結合配列にそれぞれ変異を導入しても，プロモーター活性の低下はあまり認められないが，両方に変異を導入すると約25%まで低下すること，2) さらに，NF-κB結合配列に変異を導入すると，LPS刺激による誘導プロモーター活性がほぼ消失することから，この3種類のシスエレメントが協調的かつ相補的に働くと予想される．さらに，BAECに転写因子C/EBPβ(別名NF-IL6)，C/EBPδ(別名NF-IL6β)の発現ベクターを導入したところ，C/EBPβはCOX-2プロモーター活

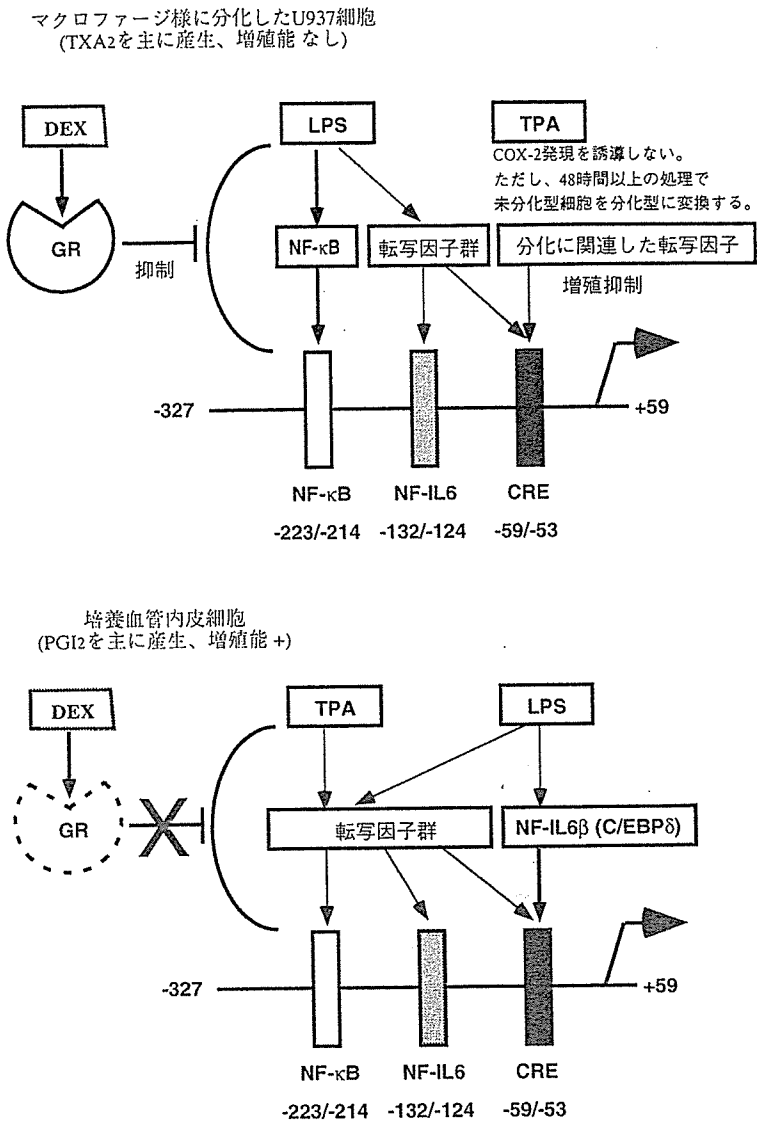

図2. マクロファージ系細胞と血管内皮細胞でのCOX-2遺伝子転写調節の比較(詳細は本文を参照). COX-2発現を誘導しない. ただし, 48時間以上の処理で未分化型細胞を分化型に変換する.

性を抑制するのに対し, C/EBPδはCREを介して促進した. 実際, LPS刺激でC/EBPδmRNAがCOX-2mRNAの誘導に先立って一過性に誘導されることから, LPS刺激によるCOX-2の誘導には新しく合成されるC/EBPδが重要であった[21]. なお, ホルボールエステル(TPA)刺激したBAECやLPS刺激したU937細胞においてもCOX-2の転写活性が上昇するが, これらの場合にはC/EBPδの誘導は観察されず, C/EBPδの発現は刺激剤特異的かつ細胞特異的であった. C/EBPδを介するCOX-2誘導のその他の例として, マウス皮膚がんにおけるCOX-2の発現亢進にC/EBPδの発現が関与することが報告された[42]. 一方, ゴナドトロピンによる卵巣でのCOX-2発現が一過性の誘導として観察されるのに対し[43], C/EBPβ欠損マウスでは誘導後の下方制御が観察されず, C/EBPβがCOX-2プロモーター活性に対して抑制することを示している[44]. 以上, 転写因子C/EBPβやC/EBPδのCOX-2遺伝子に対する効果は, 他の転写因子より遅れて働くことが示唆された. また, ヒトCOX-2のCREの配列はランダムセレクション法で同定されたC/EBPδの配列と相同性が高く, パリンドローム構造を持つ典型的なCREとは異なっていた[45].

なおCOX-2の発現調節に関しては, 我々以外にも多数の報告がある[46)-48]. その中で最近, 1) マクロファージにおいても異なった転写因子が時間軸に沿ってCOX-